Article

Neuron

Loss of Nardilysin, a Mitochondrial Co-chaperone for α-Ketoglutarate Dehydrogenase, Promotes mTORC1 Activation and Neurodegeneration

Highlights

- NRD1 binds to and chaperones OGDH (α-KGDH) in mitochondria
- Loss of NRD1 or OGDH leads to a progressive neurodegeneration
- Loss of NRD1 or OGDH increases α-KG, elevates mTORC1 activity, and impairs autophagy
- Rapamycin alleviates neuronal defects resulting from reduced NRD1 or OGDH function

Authors

Wan Hee Yoon, Hector Sandoval, Sonal Nagarkar-Jaiswal, ..., Ender Karaca, James R. Lupski, Hugo J. Bellen

Correspondence

hbellen@bcm.edu

In Brief

Yoon et al. show that the proper folding of oxoglutarate dehydrogenase (OGDH), the Krebs cycle enzyme, requires Nardilysin (NRD1) in the mitochondria. Loss of *Nrd1* or *Ogdh* causes an elevated level of α-ketoglutarate, which leads to neurodegeneration by promoting mTORC1 activity and reducing autophagy.

Yoon et al., 2017, Neuron *93*, 115–131
January 4, 2017
http://dx.doi.org/10.1016/j.neuron.2016.11.038

CellPress

Neuron
Article

Loss of Nardilysin, a Mitochondrial Co-chaperone for α-Ketoglutarate Dehydrogenase, Promotes mTORC1 Activation and Neurodegeneration

Wan Hee Yoon,[1,2] Hector Sandoval,[2] Sonal Nagarkar-Jaiswal,[1,2] Manish Jaiswal,[1,2] Shinya Yamamoto,[2,3,4] Nele A. Haelterman,[3] Nagireddy Putluri,[5] Vasanta Putluri,[5] Arun Sreekumar,[5] Tulay Tos,[6] Ayse Aksoy,[7] Taraka Donti,[2] Brett H. Graham,[2,3] Mikiko Ohno,[8] Eiichiro Nishi,[8] Jill Hunter,[9] Donna M. Muzny,[10] Jason Carmichael,[11] Joseph Shen,[11] Valerie A. Arboleda,[12] Stanley F. Nelson,[12] Michael F. Wangler,[2,3,4] Ender Karaca,[2] James R. Lupski,[2,10,13] and Hugo J. Bellen[1,2,3,4,14,15,*]

[1]Howard Hughes Medical Institute
[2]Department of Molecular and Human Genetics
[3]Program in Developmental Biology
Baylor College of Medicine, Houston, TX 77030, USA
[4]Jan and Duncan Neurological Research Institute, Texas Children's Hospital, Houston, TX 77030, USA
[5]Department of Molecular and Cellular Biology and Advanced Technology Core, Baylor College of Medicine, Houston, TX 77030, USA
[6]Department of Medical Genetics
[7]Department of Child Neurology
Dr. Sami Ulus Research and Training Hospital of Women's and Children's Health and Diseases, Ankara 06080, Turkey
[8]Department of Cardiovascular Medicine, Graduate School of Medicine, Kyoto University, Sakyo-ku, Kyoto 606-8507, Japan
[9]Department of Pediatric Radiology, Texas Children's Hospital and Department of Radiology
[10]Human Genome Sequencing Center
Baylor College of Medicine, Houston, TX 77030, USA
[11]Medical Genetics and Metabolism, Valley Children's Hospital, Madera, CA 93636, USA
[12]Departments of Human Genetics and Pathology and Laboratory Medicine, David Geffen School of Medicine, University of California, Los Angeles, CA 90095, USA
[13]Department of Pediatrics, Texas Children's Hospital
[14]Department of Neuroscience
Baylor College of Medicine, Houston, TX 77030, USA
[15]Lead Contact
*Correspondence: hbellen@bcm.edu
http://dx.doi.org/10.1016/j.neuron.2016.11.038

SUMMARY

We previously identified mutations in *Nardilysin* (*dNrd1*) in a forward genetic screen designed to isolate genes whose loss causes neurodegeneration in *Drosophila* photoreceptor neurons. Here we show that NRD1 is localized to mitochondria, where it recruits mitochondrial chaperones and assists in the folding of α-ketoglutarate dehydrogenase (OGDH), a rate-limiting enzyme in the Krebs cycle. Loss of *Nrd1* or *Ogdh* leads to an increase in α-ketoglutarate, a substrate for OGDH, which in turn leads to mTORC1 activation and a subsequent reduction in autophagy. Inhibition of mTOR activity by rapamycin or partially restoring autophagy delays neurodegeneration in *dNrd1* mutant flies. In summary, this study reveals a novel role for NRD1 as a mitochondrial co-chaperone for OGDH and provides a mechanistic link between mitochondrial metabolic dysfunction, mTORC1 signaling, and impaired autophagy in neurodegeneration.

INTRODUCTION

Mitochondria are essential organelles for all metazoans, and defects of mitochondrial function are implicated in metabolic and neurodegenerative diseases (Pickrell and Youle, 2015; Rustin et al., 1997). The mechanisms leading to degeneration are often associated with elevated reactive oxygen species (ROS) or decreased ATP production due to defects in the electron transport chain (ETC) (Johri and Beal, 2012). However, mitochondria also play a critical role in metabolism via the Krebs or TCA cycle. Among the TCA cycle metabolites, α-ketoglutarate (α-KG or 2-oxoglutarate) lies at the intersection between carbon and nitrogen metabolism where it plays an important role in nutrition sensing and metabolic homeostasis (Huergo and Dixon, 2015). α-KG, together with glutamine, has been shown to regulate mechanistic target of rapamycin (mTOR) activity and autophagy (Chin et al., 2014; Durán et al., 2012).

α-KG is produced from isocitrate by isocitrate dehydrogenase 2 and 3 (IDH2/3) and is oxidized by the α-ketoglutarate dehydrogenase complex (α-KGDHc) to succinyl-CoA in mitochondria. α-KGDHc consists of three different enzymes, including 2-oxoglutarate dehydrogenase (OGDH). Enzyme complexes consisting of multiple units in mitochondria are thought to require molecular chaperones or assembly factors since each unit

imported from the cytosol into the mitochondria needs to be properly folded and protected from aggregation until assembled into a complex. For example, succinate dehydrogenase assembly factors (SDHAFs) are required for succinate dehydrogenase (SDH) complex function (Na et al., 2014; Van Vranken et al., 2014). No assembly factor, however, has yet been identified for chaperoning enzymes in α-KGDHc.

We identified mutations in *Drosophila Nardilysin* (*N-arginine dibasic convertase*; *dNrd1*) in an unbiased forward genetic screen designed to identify genes whose loss of function causes neurodegeneration (Yamamoto et al., 2014). NRD1 belongs to the family of zinc-metalloendopeptidases that cleave doublets of basic amino acids at the N-terminal side of arginine residue of neuropeptides in vitro (Chesneau et al., 1994; Pierotti et al., 1994). In vertebrates, NRD1 has been shown to localize to different cellular compartments, including the cell surface, nucleus, and cytosol in different cells or tissues (Hiraoka et al., 2014; Hospital et al., 2000; Ma et al., 2004) NRD1 has multiple functions, including ectodomain shedding of cell surface proteins and transcriptional coregulation in the nucleus (Hiraoka et al., 2014; Nishi et al., 2006; Ohno et al., 2009).

In mammals, NRD1 is expressed in the brain (Fumagalli et al., 1998) and loss of *mNrd1* in mice causes prenatal growth defects and neonatal lethality (Ohno et al., 2009). Some mutant mice escape neonatal death and live for about 2 years. However, these escapers show a slow progressive neurodegeneration, enhanced limb-clasping reflexes, impaired motor activity, cognitive deficits, and hypomyelination (Ohno et al., 2009). Yet, the mechanisms underlying these phenotypes are ill defined, and how the loss of NRD1 causes the phenotypes remains unclear.

In this study, we show that NRD1 localizes to mitochondria, where it recruits mitochondrial chaperones to properly fold OGDH. We document that absence of NRD1 leads to a severe reduction of OGDH enzyme activity and elevated levels of its substrate, α-KG. Our findings also led to the identification of patients with neurodegenerative phenotypes that carry homozygous deleterious variants in *NRD1* and *OGDH-like* (*OGDHL*). Using recently developed genetic tools in *Drosophila*, we show that the proteins with these variants are not functional, suggesting that these genes may be linked to neurological disorders. Hence, we uncovered a novel factor required for chaperoning OGDH, an essential enzyme in the TCA cycle. Furthermore, we show that loss of *Nrd1* or *Drosophila Ogdh* (*dOgdh*) causes a progressive neurodegeneration and provide genetic data that link these genes to neurological conditions in human.

RESULTS

Mutations in *dNrd1* Cause a Slow Demise of Neuronal Function and Structure

To identify novel genes required for neuronal function, we performed a forward genetic screen for essential genes on the *Drosophila* X chromosome (Haelterman et al., 2014; Yamamoto et al., 2014). To assess whether these mutations cause defects in neuronal function, we performed electroretinogram (ERG) recordings in homozygous mutant clones in the eye. We isolated four nonsense mutations in *CG2025* that cause pupal lethality, fail to complement each other (Figure S1A), and cause similar phenotypes in ERG assays (Figures 1A–1C). *CG2025* is a *Drosophila* homolog of *NRD1* (*dNrd1*) (Figure 1E; Figure S1B). All alleles are rescued by wild-type (WT) genomic transgenes (Venken et al., 2009, 2010) or ubiquitous expression of *dNrd1* cDNA (Figure S1C).

dNrd1 mutants exhibit a slow progressive loss of ERG on- and off-transients and a decrease in amplitude when compared to controls (Figures 1A–1C). Since on- and off-transients are a measure of synaptic transmission between the photoreceptor cells (PRs) and the postsynaptic neurons (Verstreken et al., 2003), these data suggest a progressive loss of synaptic transmission in *dNrd1* mutants.

To assess whether *dNrd1* loss is associated with morphological defects, we sectioned the retinae of 1-day-old adult flies with *dNrd1* mutant clones. As shown in Figure 1D, $dNrd1^{A}$ exhibits subtle defects in young flies, and 35-day-old mutant clones exhibit gross morphological abnormalities with loss of numerous PRs (Figure 1D). Therefore, mutations in *dNrd1* cause subtle developmental defects and display a striking progressive age-dependent demise of PRs.

NRD1 Is a Mitochondrial Protein

To unravel the mechanism by which loss of NRD1 causes defects in neuronal maintenance, we examined the subcellular localization of NRD1. NRD1 has been reported to localize to the cell surface, cytoplasm (Hospital et al., 2000), and nucleus (Ma et al., 2004). As our X chromosome screen led to the isolation of more than 30 nuclear-encoded genes that cause neurodegeneration and encode proteins targeted to mitochondria (Yamamoto et al., 2014), we analyzed *Drosophila* NRD1 (DNRD1) sequence using MitoProt (Claros and Vincens, 1996) and noted that it contains a putative mitochondrial targeting sequence (MTS) in the N-terminal 42 amino acids (Figure 1E). Similarly, vertebrate NRD1s also contain MTSs (Figure 1E).

To test whether DNRD1 is localized to mitochondria, we expressed a C-terminally V5-tagged DNRD1 (DNRD1-V5) in Schneider 2 (S2) cells expressing mito-GFP (Rizzuto et al., 1995) and found that DNRD1-V5 colocalized with mito-GFP (Figure 2A). Similarly, DNRD1-V5 expressed in fly muscles (Figure 2B) or neurons (Figure 2C) also colocalizes with ATP5A, the α subunit of mitochondrial complex V, or with mito-GFP. C-terminally V5-tagged human NRD1 (NRD1-V5) also colocalizes with mito-GFP in S2 cells and fly muscles (Figures 2D and 2E). However, fly or human NRD1s lacking MTS (NRD1-ΔMTS) fail to localize to mitochondria in S2 cells (Figures 2A and 2D). Interestingly, a small fraction of DNRD1-ΔMTS colocalizes with mitochondrial markers in muscles of *dNrd1* mutants (Figure 2B), suggesting that other sequences within DNRD1 may also participate in mitochondria targeting of DNRD1 in vivo.

Finally, we tested whether substitution of an alanine residue for the glutamate residue required for the catalytic Zn^{2+} binding (E161A) affects protein localization. As shown in Figure S2, this point mutation alters the protein localization in S2 cells and muscles, resulting in cytoplasmic localization. In summary, our data show that both DNRD1 and human NRD1 localize to mitochondria (Figures 2A–2E).

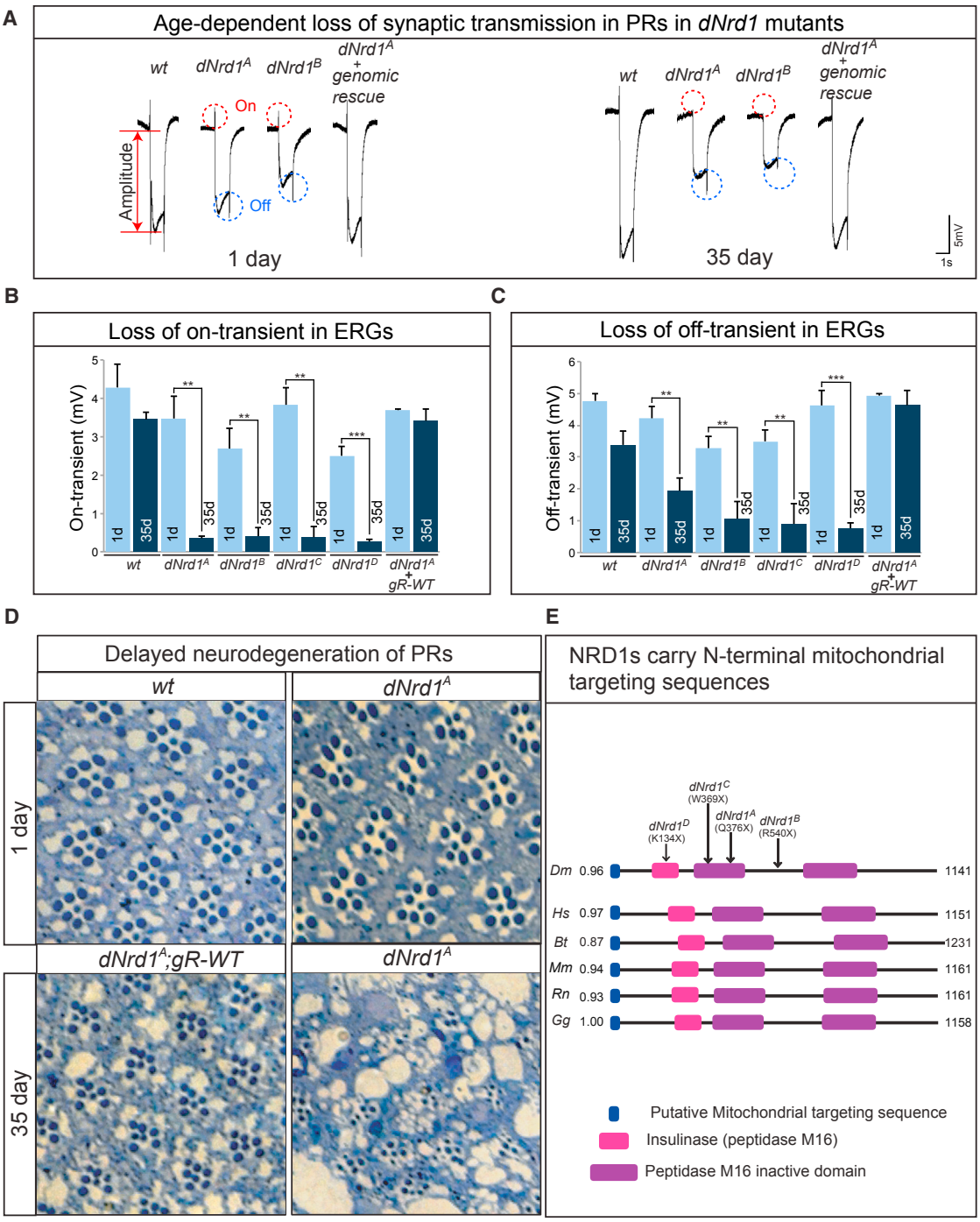

Figure 1. *dNrd1* Mutants Exhibit Progressive Neurodegenerative Features in PRs

(A) ERGs of 1-day-old and 35-day-old mutant clones in PRs of wild-type (WT), four *dNrd1* alleles ($dNrd1^{A, B, C, and D}$), and $dNrd1^{A}$ mutants carrying an 80 kb P[acman] genomic rescue transgene (*gR-WT*). An ERG trace consists of an on-transient (red dotted circles), an amplitude (red arrow), and an off-transient (blue dotted circles).

(B and C) Quantification of the on-transients (B) and off-transients (C) of ERG traces in (A). Error bars indicate SEM. p values were calculated using Student's t test. **p < 0.01, ***p < 0.001.

(D) Light micrographs of cross sections of retina of 1-day-old and 35-day-old flies in WT, $dNrd1^{A}$, and $dNrd1^{A}$; *gR-WT*.

(E) Schematic of protein domains of fly and vertebrate NRD1. Arrows indicate molecular lesions and alleles of *dNrd1*. Blue boxes indicate mitochondria targeting sequences (MTSs) predicted by MitoProt and numbers beside the blue boxes indicate the probability that each NRD1 localizes to the mitochondria. Abbreviations: *Dm*, *Drosophila melanogaster*; *Hs*, *Homo sapiens*; *Bt*, *Bos taurus*; *Mm*, *Mus musculus*; *Rn*, *Rattus norvegicus*; *Gg*, *Gallus gallus*. See also Figure S1.

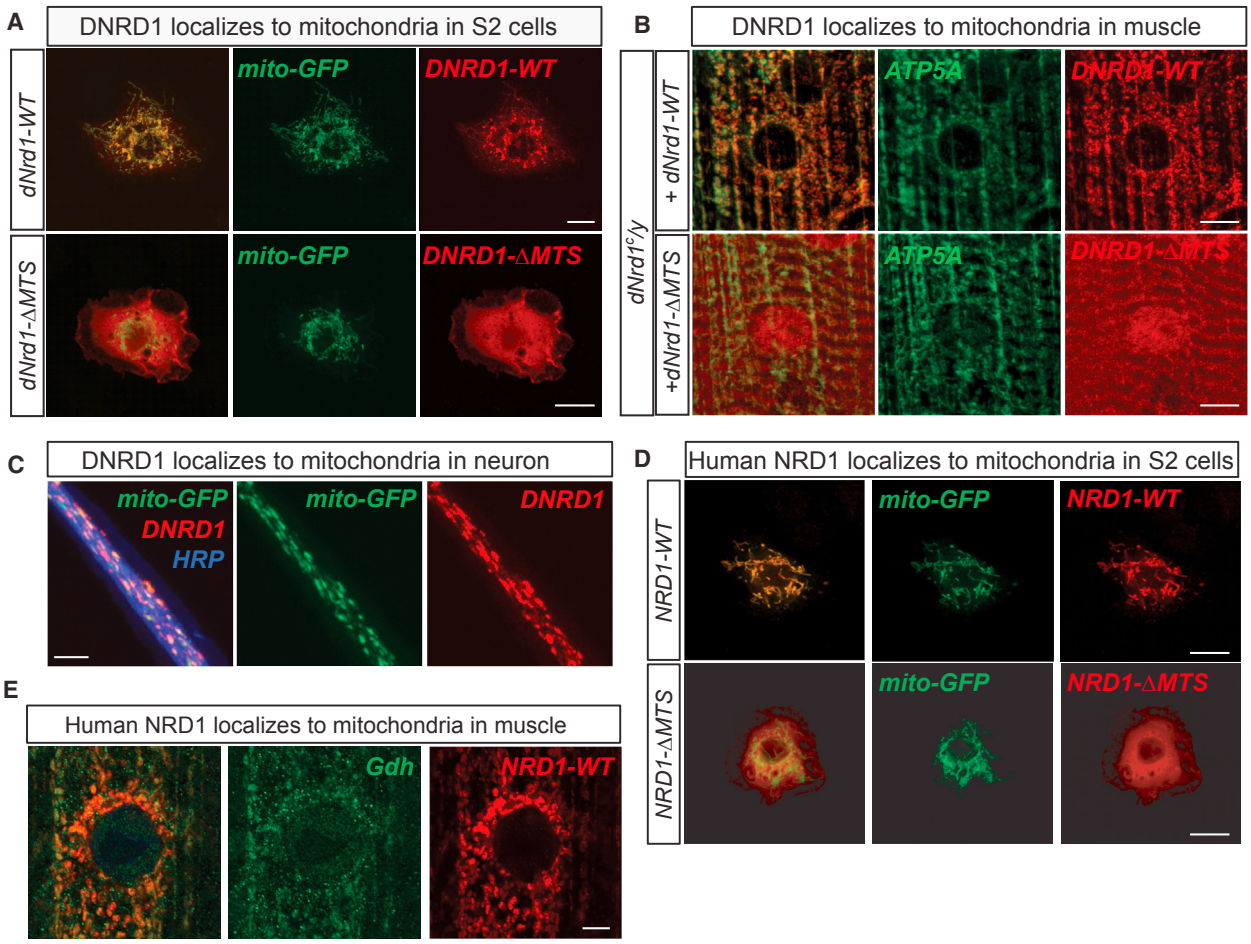

Figure 2. NRD1 Localizes to the Mitochondria

(A) Confocal micrographs of S2 cells co-expressing mito-GFP (green) and full-length V5-tagged *dNrd1* (DNRD1-WT) or V5-tagged *dNrd1* cDNA lacking N-terminal MTS (DNRD1-ΔMTS) (red). Scale bars, 10 μm.

(B) Confocal micrographs of *dNrd1*^{C} mutant larvae muscle expressing *dNrd1*-V5 (DNRD1-WT) or *dNrd1-ΔMTS-V5* (DNRD1-ΔMTS) (red), using a muscle driver (*C57-Gal4*). ATP5A (green) labels mitochondria. Scale bars, 10 μm.

(C) Confocal micrographs of motor neuron axons co-expressing mito-GFP (green) and *dNrd1*-V5 (red) (*D42-GAL4* > *UAS-dNrd1-V5*, *UAS-mito-GFP*). Scale bar, 5 μm.

(D) Confocal micrographs of S2 cells co-expressing mito-GFP (green) and V5-tagged full-length human *NRD1* (*NRD1-WT*) or *NRD1* cDNA lacking N-terminal MTS (*NRD1-ΔMTS*) (red). Scale bars, 10 μm.

(E) Confocal micrographs of *dNrd1*^{A} mutant larvae muscle expressing *human NRD1* (red) (*da-Gal4* > *UAS-human NRD1-V5*). Gdh (green) labels mitochondria. Scale bars, 5 μm. See also Figure S2.

Loss of NRD1 Does Not Affect ATP and ROS Production

Failure to control ATP production, mitochondrial biogenesis or dynamics, as well as many other lesions of mitochondrial proteins, are associated with neurodegenerative diseases (Burté et al., 2015; Johri and Beal, 2012; Pickrell and Youle, 2015). We, therefore, assessed basic mitochondrial properties in *dNrd1* mutant tissues. We did not observe obvious differences in mitochondrial DNA (mtDNA) copy number (Figure 3A) or abundance of numerous mitochondrial proteins between *dNrd1* mutants and controls (Figure 3B). In addition, *dNrd1* mutants exhibit a normal mitochondrial membrane potential (Figure 3C). Moreover, NADH levels in *dNrd1* mutants are very similar to those observed in controls (Figure 3D). Furthermore, ATP levels in *dNrd1* mutants are not different from controls (Figure 3E). In addition, the activity of Aconitase, an enzyme that is sensitive to ROS, is not altered in *dNrd1* mutants (Figure 3F). However, the activities of the ETC complexes I, III, and IV are increased about 2-fold compared to controls (Figure 3G), but complex II activity is not significantly altered (Figure 3G). These data indicate that total energy production is not altered in *dNrd1* mutants but suggest that a compensatory upregulation of complexes I, III, and IV activities may mask potential defects in energy production.

Loss of NRD1 Affects Metabolites of the TCA Cycle

The lack of obvious mitochondrial phenotypes associated with the loss of *dNrd1* prompted us to explore metabolites in *dNrd1*

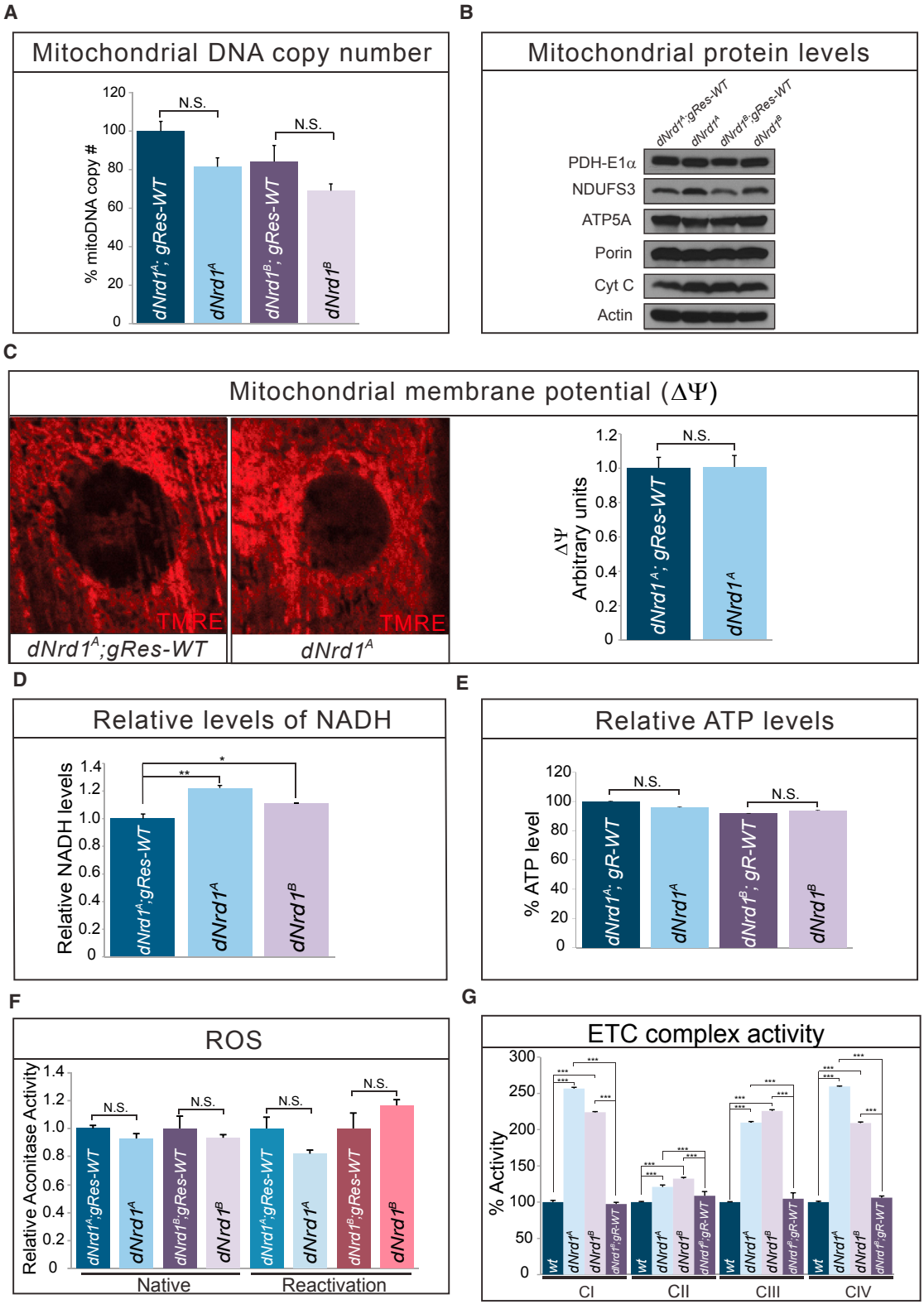

Figure 3. Loss of *dNrd1* Does Not Interfere with ATP Levels

(A) Relative amount of mitochondrial DNA copy number measured in *dNrd1* mutant larvae and controls.

(B) Western blots for mitochondrial proteins—PDH-E1α, NDUFS3, ATP5A, Porin, Cyt C, and Actin in *dNrd1* mutants and controls.

(legend continued on next page)

mutant animals. The most obvious defect that we observed was a dramatic increase in α-KG and glutamine in *dNrd1* mutants (Figure 4A). Similarly, mouse embryonic fibroblasts (MEFs) that lack NRD1 (Ohno et al., 2009) also exhibit a significant accumulation of α-KG and glutamine (Figure 4B). Our data suggest that when NRD1 is lost, the activity or levels of enzymes of the α-KGDHc are reduced, leading to the accumulation of its substrate, α-KG (Figure 4L). An accumulation of α-KG may lead to an increase in glutamine in *dNrd1* mutants and mutant MEFs through cataplerosis, a process that attempts to deplete the pool of α-KG by converting it into glutamine (Owen et al., 2002).

NRD1 Is Required for the Activity of OGDH

To determine the cause of α-KG accumulation, we examined the enzymatic activity of *Drosophila* OGDH, along with other TCA cycle enzymes in *dNrd1* mutants. As shown in Figure 4C, loss of *dNrd1* leads to a severe loss of the OGDH activity, whereas the activity of other enzymes in the TCA cycle are not affected or are mildly affected in *dNrd1* mutants when compared to controls (Figures 3F and 4D–4F). These results indicate that loss of *dNrd1* affects the stability, abundance, or enzymatic activity of OGDH.

To measure the protein level of DOGDH in *dNrd1* mutants in vivo, we took advantage of the presence of a MiMIC (Minos-mediated integration cassette) transposon inserted in a coding intron of *dOgdh* (Nagarkar-Jaiswal et al., 2015; Venken et al., 2011) (Figure S3A). We generated a fly strain in which the MiMIC transposon was replaced with an artificial exon encoding GFP. As shown in Figure S3B, the internally tagged DOGDH-GFP protein localizes to the mitochondria and co-localizes with ATP5A. To test whether the loss of *dNrd1* affects DOGDH protein levels, we generated *dNrd1* mutants carrying *dOgdh-GFP*. *dNrd1* mutants exhibit a dramatic decrease of the protein levels of DOGDH-GFP, both in total lysate and in the mitochondrial fraction when compared to controls, whereas the level of ATP5A in the mutants is comparable to controls (Figure 4G). To test whether DNRD1 regulates the level of other enzymes in the TCA cycle, we compared the level of malate dehydrogenase 2 (MDH2) in *dNrd1* mutants with that of controls and found that they are similar (Figure 4H). Therefore, DNRD1 is required for the activity and proper protein levels of DOGDH in *Drosophila*.

To assess the levels and activity of OGDH in the absence of NRD1 in mammalian cells, we compared the expression of OGDH in $mNrd1^{-/-}$ MEFs to that in control $mNrd1^{+/+}$ MEFs. Since the levels of α-KG are elevated in $mNrd1^{-/-}$ MEFs, we expected a loss of OGDH. Surprisingly, the level of OGDH protein in $mNrd1^{-/-}$ MEFs is elevated compared to wild-type MEFs, whereas the levels of citrate synthase (CS) are similar in mutant and wild-type MEFs (Figure 4I). However, the enzymatic activity of OGDH in $mNrd1^{-/-}$ MEFs is severely reduced compared to wild-type MEFs (Figure 4J), consistent with an elevation in α-KG (Figure 4B). These data suggest that, in mammalian cells, NRD1 is required for the activity of OGDH, similar to flies, but not for abundance of OGDH. Nevertheless, our data demonstrate that NRD1 is required for the proper function of OGDH in flies and mice.

Loss of *dOgdh* Phenocopies *dNrd1* Mutants

If OGDH is the major target of NRD1 in vivo, we anticipated that reduction of *dOgdh* would phenocopy the loss of *dNrd1*. Knockdown of *dOgdh* via RNAi in larvae causes a dramatic increase in α-KG and glutamine (Figure 4K) similar to and more severe than the *dNrd1* mutant (Figure 4A), suggesting that DOGDH activity is incompletely lost in *dNrd1* mutants, consistent with the enzymatic assays (Figure 4C). Additionally, the profile of amino acid changes, including elevated lysine level in $mNrd1^{-/-}$ MEFs, are similarly observed in *dOgdh* knockdown flies (Figures S4A and S4B). Moreover, knockdown of *dOgdh* in PRs causes a slow progressive loss of synaptic transmission (Figure S4C), similar to the ERG phenotypes seen in *dNrd1* mutant clones (Figures 1A–1C). Altogether, these data reveal that OGDH is a major target of NRD1 in vivo and that loss/reduction of function of the two proteins have similar metabolic and neurologic phenotypes.

NRD1 Interacts with OGDH as well as Numerous Mitochondrial Chaperones

To further determine the role of NRD1, we sought to identify proteins that physically interact with NRD1. We performed immunoprecipitation (IP) mass spectrometry (MS) of V5-tagged DNRD1 and identified numerous mitochondrial proteins, including *Drosophila* OGDH (DOGDH) (Figure 5A; Figure S5A; Table S1). The interaction between DNRD1 and DOGDH was confirmed via co-IP in S2 cells (Figure 5B). Interestingly, 20 out of 60 proteins with spectral counts of 9-fold or more in DNRD1-V5-expressing samples when compared to controls were associated with mitochondria (Figure 5A). Bioinformatics analyses based on STRING (http://string-db.org/) (Franceschini et al., 2013) and COMPLEAT (http://www.flyrnai.org/compleat/) (Vinayagam et al., 2013) revealed that 10 of the 20 mitochondrial proteins can be assigned to three different functional categories (Figure S5B). These include mitochondrial chaperones (L(2)tid/DNAJA3; Roe1/GRPEL1; Hsc70-5/HSPA9; Hsp60C/HSP60; CG3731/PMPCB), enzymes of the TCA cycle (DOGDH/OGDH; CG6439/IDH3B; Gdh/GLUD1), and proteins involved in amino acid catabolism (CG2118/MCCC1; CG3267/MCCC2) (Figure S5B). In addition, two other proteases that also function as chaperones (Lon/LonP1; CG4538/CLPX) interact with DNRD1 (Figure 5A). We verified the interaction between DNRD1 and Hsc70-5, L(2)tid and Hsp60 in S2 cells (Figure 5C). Given that DNRD1 can interact with DOGDH and a number of mitochondrial chaperone proteins, NRD1 may help chaperone OGDH.

(C) Mitochondrial membrane potential is measured by TMRE dye in larva muscle (left). Quantification of membrane potential in $dNrd1^{A}$ mutant and control (right).
(D) Relative levels of NADH in *dNrd1* mutants and control.
(E) Relative levels of ATP in *dNrd1* mutants and controls.
(F) Aconitase activity in both native and reactivation conditions in *dNrd1* mutant larvae and controls.
(G) The ETC complex activity (I–IV) in *dNrd1* mutant larvae and controls. Errors bars in (A), (C), (D), (E), (F), and (G) indicate SEM. p values were calculated using Student's t test. *$p < 0.05$, **$p < 0.01$, ***$p < 0.001$. n.s. indicates not statistically significant.

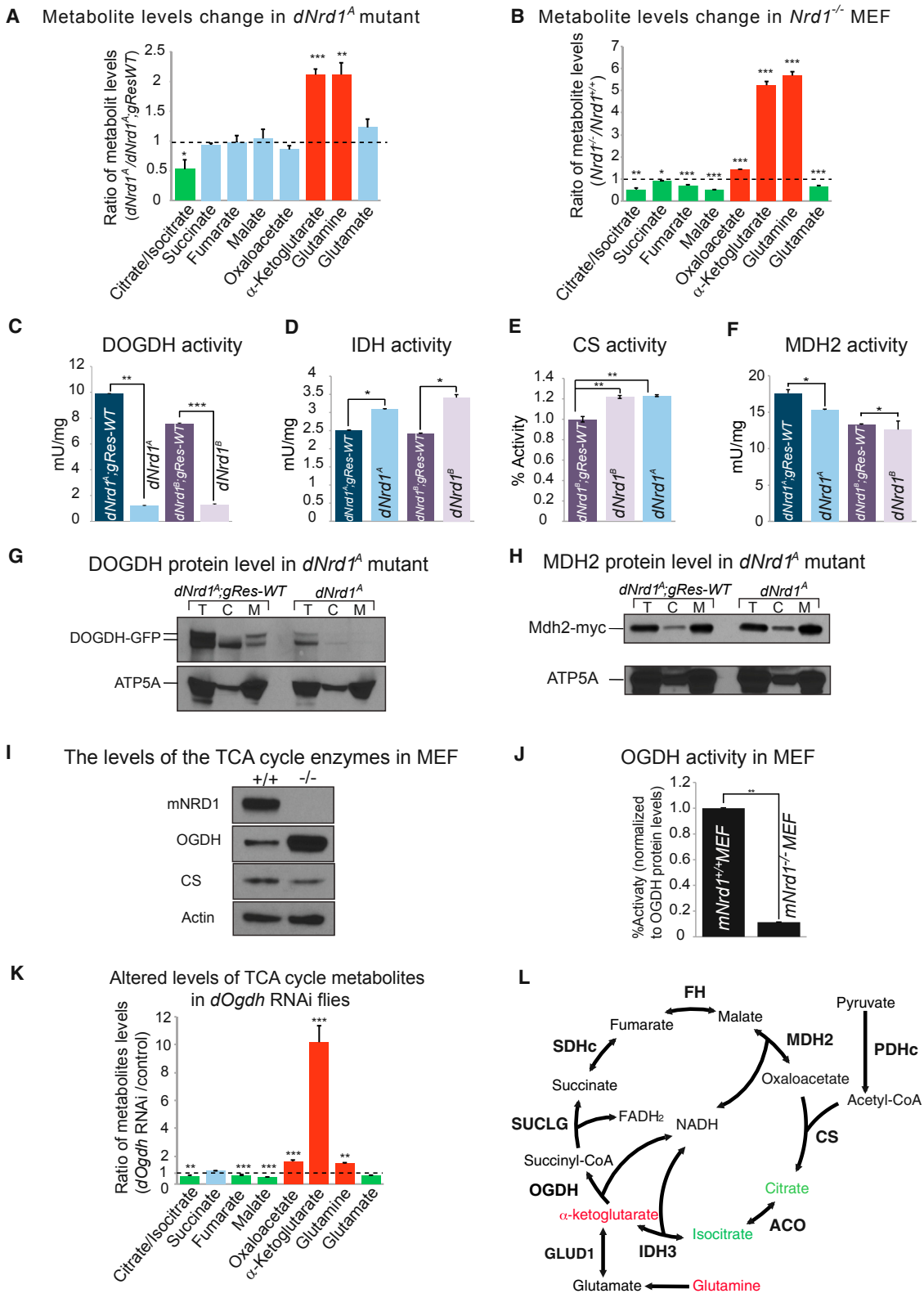

Figure 4. NRD1 Is Required for the Activity of OGDH

(A) Quantification of ratio of metabolites in the TCA cycle of *dNrd1*^{A} mutants to those in control larvae.

(B) Quantification of ratio of metabolites in the TCA cycle of *Nrd1*^{KO} mutant MEF (*mNrd1*$^{-/-}$) to those in wild-type MEF (*mNrd1*$^{+/+}$).

(legend continued on next page)

NRD1 Recruits Mitochondrial Chaperones for OGDH

The interaction between DNRD1 with DOGDH and mitochondrial chaperones when combined with a dramatic decrease in activity of DOGDH in the absence of DNRD1 suggests that DNRD1 is required for proper mitochondrial import, folding, and/or stabilization of DOGDH (Figure 5H). Similarly, an increase in OGDH protein levels in *mNrd1*$^{-/-}$ MEFs combined with a severe decrease in OGDH activity also suggests that the folding of the protein may be impaired. However, unlike in flies, the protein is not degraded and leads to an accumulation of OGDH (Figure 4I).

As DNRD1 interacts with Hsc70-5 and Roe1, two subunits of the presequence translocase-associated motor (PAM) complex in the inner mitochondria (Pfanner et al., 1997) (Figures 5A and 5H; Figure S5B), we performed a mitochondrial import assay in which in vitro translated DOGDH protein was mixed with purified mitochondria (Horwich et al., 1985). C-terminally Flag-tagged DOGDH protein (DOGDH-Flag) produced by in vitro transcription and translation was incubated with mitochondria purified from either *dNrd1* mutant or control animals. Upon incubation for different time periods, the mitochondria were isolated and washed with buffer containing protease inhibitors. Western blots allowed assessment of the abundance of DOGDH in mitochondria. The data indicate that the protein is imported into mitochondria and that the levels are maximal after 20 min in controls (Figure 5D). At early time points (Figure 5D; 2 and 5 min), the amount of imported DOGDH protein in *dNrd1* mutant and control mitochondria is similar, suggesting that mitochondrial import is not defective in the absence of DNRD1 (Figure 5D). However, imported DOGDH protein is gradually lost in *dNrd1* mutant mitochondria (Figure 5D). These data indicate that DNRD1 is not required for the import of DOGDH but is essential for the stability of newly imported DOGDH in mitochondria.

The loss of DOGDH in mitochondria in the absence of DNRD1 suggests that DOGDH is misfolded and degraded. MDJ1, a yeast homolog of L(2)tid, is required for the folding of newly imported proteins in the mitochondrial matrix (Rowley et al., 1994). We find that L(2)tid protein enhances the physical interaction between DNRD1 and DOGDH proteins (Figure 5E), but other chaperones did not promote this interaction. This suggests that DNRD1, DOGDH, and L(2)tid form a complex and may assist in the proper folding of DOGDH.

Misfolded mitochondrial proteins typically precipitate more easily than native proteins (Bender et al., 2011). We, therefore, sought to examine whether the solubility of DOGDH is affected in *dNrd1* mutants in response to heat shock. Since DOGDH is significantly reduced in *dNrd1* mutants (Figure 4G), we overexpressed DOGDH in wild-type and mutant larvae. Purified mitochondria expressing DOGDH-Flag from control or *dNrd1* mutant animals were incubated at 25°C or 42°C. Upon 10 min incubation, the mitochondria were lysed with detergent-containing buffer, and soluble and insoluble fractions were separated by ultracentrifugation. In control mitochondria, DOGDH-Flag was not detected in the pellet fraction, whereas in *dNrd1* mutant mitochondria, a significant fraction of DOGDH-Flag was observed in the pellet at 42°C (Figure 5F). In contrast, the solubility of ATP5A that served as a negative control is much less affected than DOGDH. These data indicate that NRD1 protects OGDH from denaturation upon heat shock.

To confirm the above results, we developed a mitochondrial chaperone assay that allows us to monitor a folding state of OGDH by measuring luciferase activity of a DOGDH-*Renilla* luciferase fusion protein (DOGDH-Rluc). Indeed, overexpression of *dNrd1* in S2 cells significantly increases DOGDH-Rluc activity (Figure 5G), suggesting that NRD1 may help fold or stabilize OGDH. To test whether NRD1 is capable of protecting OGDH from stress (holdase activity) or refolding denatured OGDH (foldase activity) (Ali et al., 2016), we incubated S2 cells in which DOGDH-Rluc is expressed with or without DRND1 at 42°C for 15 min and returned the cells to 21°C for 3 hr. Immediately after the 42°C for 15 min shift, S2 cells expressing DNRD1 exhibit a higher DOGDH-Rluc activity compared to control (Figure 5G), indicating that NRD1 can protect OGDH from the heat shock and has a holdase activity. However, after a 3 hr recovery, S2 cells expressing DNRD1 do not show higher DOGDH-Rluc activity when compared to controls, indicating that NRD1 lacks foldase activity. Altogether, these data suggest that NRD1 forms a complex with mitochondrial chaperones to fold imported OGDH in native condition and protect OGDH from denaturation under stress condition (Figure 5H).

Patients with Homozygous Variants in *NRD1* and *OGDHL* Develop Severe Neurological Features

Since loss of *dNrd1* or *dOgdh* causes a neurodegenerative phenotype in *Drosophila* and *mNrd1* knockout mice exhibit severe developmental and neuronal defects (Ohno et al., 2009), we hypothesized that variants in orthologous human genes may be linked to rare neurological conditions. We examined whole exome sequencing (WES) data and performed genome analyses of nearly 6,000 patients of the Baylor-Hopkins Center for Mendelian Genomics (BHCMG) database (Chong et al., 2015). We did not identify a deleterious allele for *NRD1*. However, a posting on GeneMatcher (https://genematcher.org) (Sobreira

(C–F) The activity of enzymes in the TCA cycle is measured from purified mitochondria (C, D, and F) or total larva extract (E) in *dNrd1* mutants and controls.
(G and H) Western blots for protein level of DOGDH-GFP (G) or protein level of Mdh2-myc expressed from genomic rescue transgene (H) and ATP5A in total (T), cytosolic (C), and mitochondrial (M) fraction in *dNrd1*^{A} mutant and control larvae.
(I) Western blots for protein level of OGDH, CS, and Actin in *Nrd1* mutant MEF (*mNrd1*$^{-/-}$) and wild-type MEF (*mNrd1*$^{+/+}$).
(J) The activity of OGDH in *Nrd1* mutant MEF (*mNrd1*$^{-/-}$) and wild-type MEF (*mNrd1*$^{+/+}$).
(K) Quantification of the ratio of metabolites in the TCA cycle of *dOgdh RNAi* larvae (*Act-Gal4/UAS-dOgdh RNAi*) compared to those in control larvae (*Act-Gal4/+*). Error bars indicate SEM (A–F, J, and K). p values were calculated using Student's t test. *p < 0.05, **p < 0.01, ***p < 0.001.
(L) Schematic representation of the TCA cycle. Metabolites that increase in both *dNrd1* mutant and *mNrd1*$^{-/-}$ MEF are shown in red color. Note that in *dNrd1* mutant flies (Figure 4A), *dOgdh* knockdown flies (Figure 4K), and *mNrd1* knockout MEFs (Figure 4B), there is a loss of some other metabolites (green) produced in the TCA cycle. Abbreviations: Citrate synthase, CS; Aconitase, ACO; Isocitrate dehydrogenase 3, IDH3; Oxoglutarate dehydrogenase, OGDH; Glutamate dehydrogenase, GDH; Succinate-CoA ligase, SUCLG; Succinate dehydrogenase complex, SDHc; Fumarate hydratase, FH; Malate dehydrogenase 2, MDH2; Pyruvate dehydrogenase complex, PDHc. See also Figures S3 and S4.

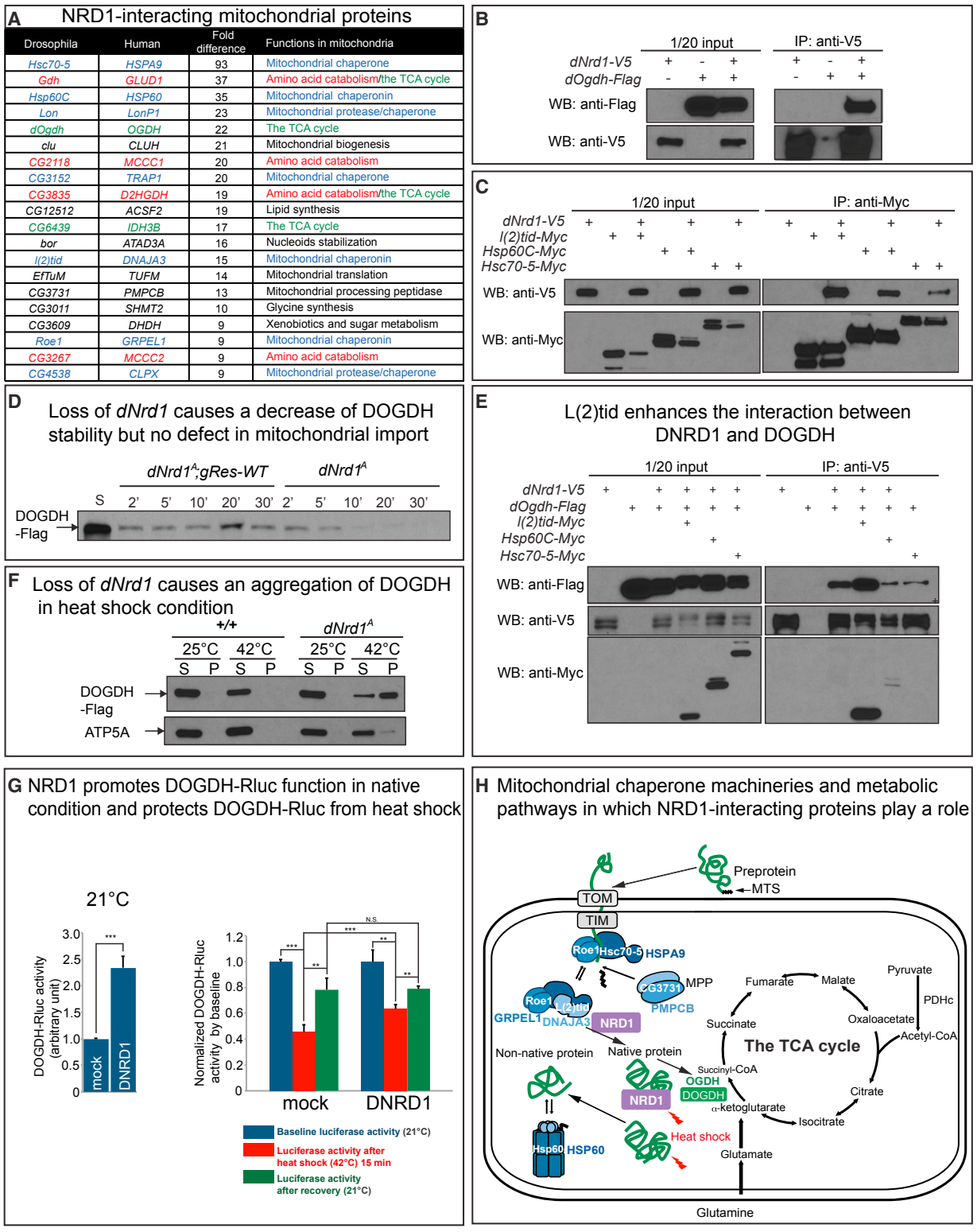

Figure 5. NRD1 Interacts with Mitochondrial Chaperones and OGDH

(A) The table shows 20 mitochondrial proteins that are identified by IP/MS using V5 antibody from DNRD1-expressing larvae (*da-Gal4* > *UAS-dNrd1-V5*). These mitochondrial proteins are selected from proteins whose spectral counts are at least 9-fold higher in DNRD1-expressing larvae compared to control (*da-Gal4*). The proteins in the TCA cycle are marked with green color, amino acid catabolism with red color, and mitochondrial chaperone proteins with blue color.

(legend continued on next page)

et al., 2015) led to the identification of a patient (CDMD1122) with severe global developmental delay and ataxia referred for clinical exome sequencing to the UCLA Clinical Genomics Center (Lee et al., 2014). The patient is homozygous for a truncating variant in *NRD1* (GenBank: NM_002525.2:exon 17:c.1906_1907delAT: p.M636VfsX2) (Figures 6A and 6B). The variant causes a frameshift leading to an M636V followed by an early termination codon. Both parents and four unaffected siblings were found to be heterozygous for this variant (Figure 6A).

We performed WES on the proband, both parents, and five unaffected siblings (Figure 6A) and did not discover any coding de novo variant in the proband. We found seven candidate genes with homozygous variants in the proband that were not present in the siblings. None of those genes have been previously associated with Mendelian disorders and six of the seven genes carry homozygous missense alleles that are predicted to be benign by multiple algorithms (Adzhubei et al., 2010; Kumar et al., 2009; Lek et al., 2016; Ng and Henikoff, 2003) (Table S2). Finally, the patient is a compound heterozygote for *OBSCN* and *PUS1*, but both variants for *OBSCN* and one of the variants of *PUS1* are classified as benign, and the clinical phenotype associated with *PUS1* does not fit the clinical phenotype of our patient (Table S2). Hence, *NRD1* is the only gene with a predicted homozygous loss-of-function allele. Truncating alleles in *NRD1* are very rare and the gene is predicted to be highly intolerant to loss-of-function mutations (pLI score of 0.88), and there are no instances of homozygous nonsense or frameshift alleles in the Exome Aggregation Consortium (ExAC) (Lek et al., 2016).

The patient had unremarkable prenatal and birth history but initially presented with developmental delay and episodes of ocular deviation in the first year of life (see Supplemental Information, "Clinical Case Histories") and developed a microcephaly (Figure 6C; Figures S6B–S6D). Altogether, the patient exhibits a progressive neurodegenerative phenotype and carries a rare, loss-of-function, homozygous truncating variant in *NRD1*.

To determine whether molecular functions of NRD1 proteins are evolutionarily conserved, we assessed whether ubiquitous expression of human *NRD1* cDNA can rescue the lethality and ERG defects associated with *dNrd1* fly mutants. The lethality and ERG defects were rescued (Figure S1C; Figure 6D), indicating that the function of NRD1 is conserved between fly and human.

Since NRD1 chaperones OGDH, we hypothesized that rare variants in homologous genes in humans may also be associated with neurological features. Humans have two homologs of *dOgdh*, *OGDH* and *OGDHL*. OGDH is widely expressed and present in most tissues while OGDHL is much more restricted in its expression pattern and mostly expressed in brain and liver (Bunik et al., 2008) (GeneCards: http://www.genecards.org/). No deleterious variants in *OGDH* or *OGDHL* have been previously reported. Within the BHCMG database, we prioritized individuals with rare homozygous or compound heterozygous variants in these genes (Chong et al., 2015). Eight individuals were selected for segregation analysis from ~6,000 individuals. Of these, seven were found to have variants with a high frequency in public databases or variants in other genes that explained their phenotype.

Among these, one undiagnosed patient (BAB4852) carries a homozygous variant in *OGDHL* (Figure 6E). This patient exhibited a severe developmental delay with cerebral and cerebellar atrophy and corpus callosum abnormality (Figure 6G). A detailed phenotypic description can be found in the Supplemental Information ("Clinical Case Histories"). The homozygous variant in *OGDHL* was considered a top candidate from a cohort of Turkish patients with brain malformations (Karaca et al., 2015). We performed WES on the proband and both parents, yielding a set of candidate variants in 13 genes, three of which are, in known disease genes, inconsistent with the phenotypes (Table S2). The homozygous variant in *OGDHL* (GenBank: NM_018245:exon18:c.C2333T:p.S778L) (Figure 6F) was predicted to be deleterious based on SIFT (Kumar et al., 2009; Ng and Henikoff, 2003) and polyphen2 (Adzhubei et al., 2010), and the gene is known to be expressed in the brain (Bunik et al., 2008) (GeneCards: http://www.genecards.org/). This variant segregates with the phenotype in the BAB4852 family as both parents and the unaffected sibling are heterozygous carriers, consistent with Mendelian expectations (Figure 6E). *OGDHL* in this patient maps within a block of absence of heterozygosity (AOH), consistent with the known consanguinity (Figure S6E). Hence, the variant in *OGDHL* was our top candidate for this patient and lack of functional data prompted us to experimentally test the functionality of the variant.

The p.S778 resides in a transketolase domain that is essential for activity of OGDHL (Figure 6F). Moreover, S778 (S793 in

(B) Co-immunoprecipitation using anti-V5 antibody from S2 cell lysates overexpressing C-terminally V5-tagged DNRD1 and C-terminally Flag-tagged DOGDH. Western blots were performed using either anti-Flag or anti-V5 antibody.

(C) Co-immunoprecipitation using anti-Myc antibody from S2 cell lysates overexpressing C-terminally V5-tagged DNRD1 and C-terminally Myc-tagged mitochondrial chaperone proteins. Western blots were performed using either anti-V5 or anti-Myc antibody.

(D) Import of C-terminally Flag-tagged DOGDH into isolated mitochondria from $dNrd1^{A}$ and control larvae. An arrow indicates DOGDH-Flag proteins detected by anti-Flag antibody. S indicates 10% of starting protein for the assay. The reactions were stopped at different time points (2, 5, 10, 20, and 30 min) after mixing mitochondria and DOGDH-Flag protein. The isolated mitochondria were subjected to western blots with anti-Flag antibody.

(E) Co-immunoprecipitation using anti-V5 antibody from S2 cell lysates overexpressing C-terminally V5-tagged DNRD1 and C-terminally Flag-tagged DOGDH, together with one of C-terminally Myc-tagged mitochondrial chaperone proteins. Western bots were performed using anti-Flag, anti-V5, or anti-Myc antibody.

(F) Mitochondria isolated from wild-type or *dNrd1* mutants expressing DOGDH-Flag (*+/Y; UAS-dOgdh-Flag /+;da-Gal4/+* or $dNrd1^{A}$*/Y; UAS-dOgdh-Flag /+;da-Gal4/+*) were incubated at the indicated temperature, and aggregated proteins were precipitated by ultracentrifugation. Supernatants (S) and pellets (P) were analyzed by western blot with an antibody against Flag or ATP5A.

(G) Mitochondrial chaperone assay of DNRD1 for DOGDH-*Renilla* luciferase (DOGDH-Rluc). In the presence of extra DNRD1, DOGDH-Rluc is ~2.2-fold more active (left), and upon heat shock, the loss of OGDH-Rluc activity is milder (right). Error bars indicate SEM. p values were calculated using Student's t test. $^{**}p < 0.01$, $^{***}p < 0.001$. n.s. indicates not statistically significant.

(H) Schematic representation of mitochondrial chaperones that play a role in import and protein folding and metabolic pathways centered in the TCA cycle. See also Figure S5.

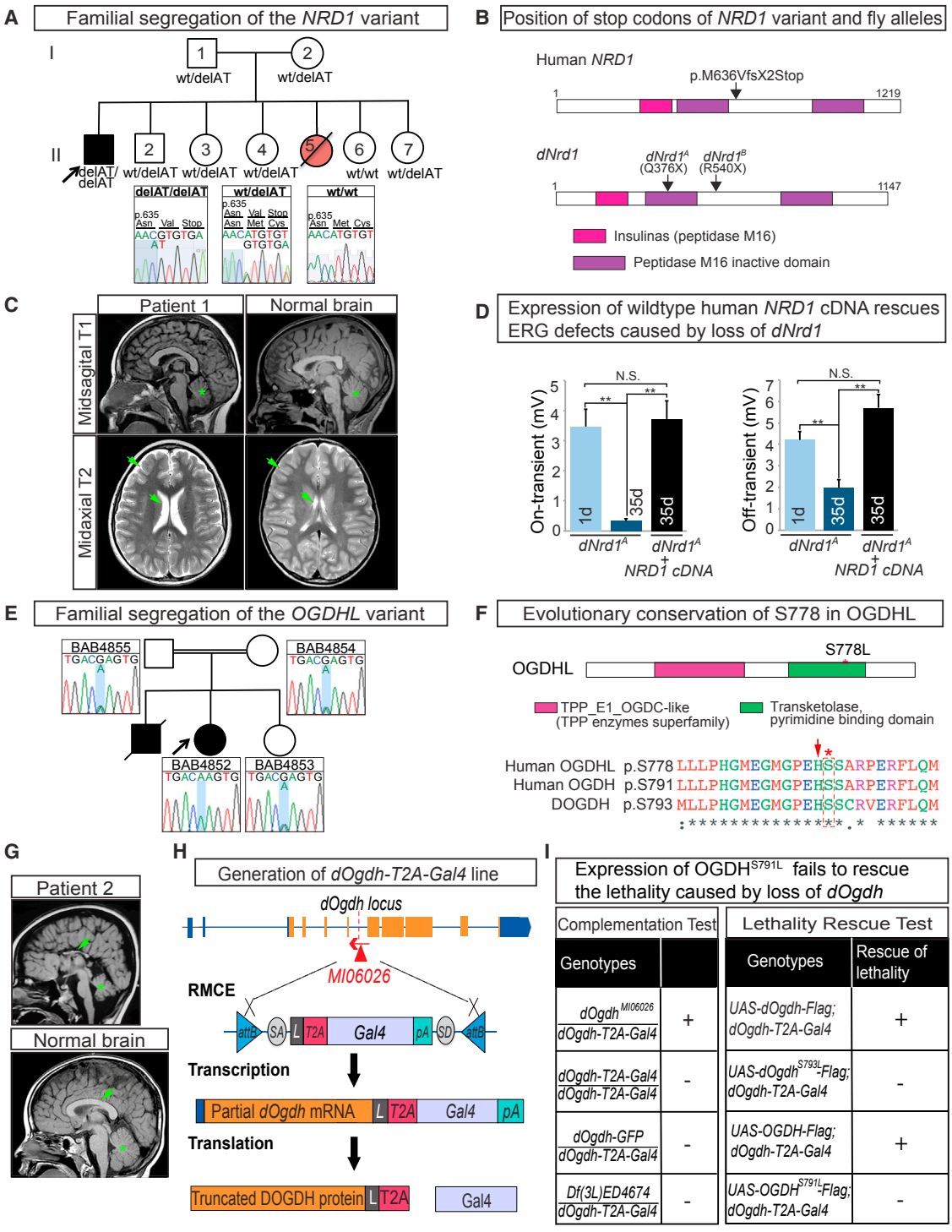

Figure 6. Identification of Patients with Neurodegenerative Phenotypes with Homozygous Deleterious Variants in *NRD1* and *OGDHL*

(A) Familial segregation of the *NRD1* variant (GenBank: NM_002525.2:exon 17:c.1906_1907delAT: p.M636VfsX2). The *NRD1* variant is homozygous in the proband and heterozygous or wild-type in the parents and unaffected siblings. A sister (red circle) was born with early onset developmental delay and failure to thrive. She died of unknown cause at 16 months of age. No additional clinical information and DNA was available.

(B) Schematic representation of protein domains of human and fly NRD1 and position of stop codons of human *NRD1* variant and fly alleles.

(C) A T1 sagittal MRI image of the patient at age 8 years showing mild cerebellar volume loss (green asterisk). A T2 midaxial image shows enlarged extracerebral spaces (green arrows) compared to those in a control MRI.

(legend continued on next page)

Drosophila) is evolutionarily conserved from bacteria to vertebrates and is adjacent to the catalytic histidine (Figure 6F, red arrow) (Bunik and Degtyarev, 2008). To assess the function of the S778L variant in flies, we created a severe loss-of-function or null allele of *dOgdh* that expresses the GAL4 gene under the control of the endogenous regulatory elements of *dOgdh* using the T2A-GAL4 system (*dOgdh-T2A-GAL4*) (Figure 6H; see Supplemental Information, "Functional Validation of a Missense Variant in *OGDHL* in Patient 2") (Bellen and Yamamoto, 2015; Diao et al., 2015; Nagarkar-Jaiswal et al., 2015). We also generated transgenes that allow expression of OGDH or OGDHL under the control of upstream activating sequence (UAS). Expression of human OGDHL did not rescue the lethality caused by loss of *dOgdh*. However, expression of human OGDH was able to rescue the lethality associated with the loss of *dOgdh*, whereas expression of $OGDH^{S791L}$ was not able to rescue (Figure 6I). In addition, expression of the fly DOGDH rescued the loss of *dOgdh*, but $DOGDH^{S793L}$ failed to rescue (Figure 6I). Moreover, the ERG defects associated with the loss of *dOgdh* were rescued by wild-type fly DOGDH, human OGDH, and OGDHL, but not with the mutant isoforms (Figure S6H). Hence, the Serine to Leucine mutation in both human and fly OGDH results in a severe loss of function.

Loss of NRD1 or OGDH Leads to Activation of TORC1 and Inhibition of Autophagy

Loss of NRD1 does not affect ATP, ROS, or mitochondrial biogenesis (Figure 3), unlike several other neurodegenerative mutants (Johri and Beal, 2012). Rather, the loss of NRD1 or its target OGDH causes a specific increase of α-KG and glutamine (Figures 4A and 4B). Interestingly, increased levels of α-KG have been documented to promote (Durán et al., 2012) or decrease TOR activity (Chin et al., 2014). We, therefore, tested whether loss of *dNrd1* or *dOgdh* affect TOR activity in fly mutants. As shown in Figures 7A and 7B, *dNrd1* mutants or *dOgdh* RNAi animals exhibit increased levels of phospho-S6 kinase (pS6K) and phospho-eukaryotic translation initiation factor 4E binding protein (p4E-BP). $Nrd1^{KO}$ ($mNrd1^{-/-}$) MEFs also exhibit an increased level in pS6K compared to control MEFs (Figure 7C), suggesting that loss of *NRD1* or *OGDH* activates mTORC1 in vivo. Unlike fly mutants, however, $Nrd1^{KO}$ ($mNrd1^{-/-}$) MEFs did not show an increase in p4E-BP levels (Figure 7C), as we observed a significant decrease of the total 4E-BP levels. Importantly, *dNrd1* mutants or *dOgdh* RNAi animals exhibit an increased level of p62, an autophagy substrate (Figures 7A and 7B), and $Nrd1^{KO}$ ($mNrd1^{-/-}$) MEFs show a decreased level in LC3B-II, an autophagy marker (Figure 7C). These data indicate that loss of *NRD1* and *OGDH* leads to mTORC1 activation, which in turn inhibits autophagy. The decrease in autophagy in $Nrd1^{KO}$ ($mNrd1^{-/-}$) MEFs is partially restored by treating the cells with rapamycin, an mTOR inhibitor (Figure 7C). Moreover, treating flies with eyes that carry *dNrd1* mutant clones or express *dOgdh* RNAi with rapamycin rescued the ERG defects (Figures 7D and 7E). These data indicate that hyperactivation of TORC1 underlies the slow progressive neurodegenerative phenotypes observed in flies.

The decrease in autophagy in *dNrd1* or *dOgdh* mutants may cause neurodegenerative phenotypes as perturbations in autophagy are associated with many neurodegenerative diseases (Menzies et al., 2015). mTORC1 activation has been shown to lead to a reduction in autophagy as well as an increase in global translation (Laplante and Sabatini, 2012). To assess whether autophagy defects cause the neurodegenerative phenotypes in vivo, we expressed low levels of *Atg1* in PRs. *Atg1* expression, a target that TOR phosphorylates, partially rescues the ERG defects caused by loss of *dNrd1* (Figure 7F). To test whether an increase in translation affects the neurodegenerative phenotypes, we expressed a dominant negative S6K (Barcelo and Stewart, 2002) that suppresses translation. This dominant negative S6K does not rescue the ERG defects (Figure S7), indicating that the reduction in autophagy and not the increase in translation, contributes to the phenotype in *dNrd1*. Hence, these data suggest that aberrant mTORC1 activation and subsequent autophagy defects promote the neurodegeneration associated with *OGDHL* and *NRD1* mutations (Figure 7G).

DISCUSSION

NRD1 Recruits Mitochondrial Chaperones to Promote OGDH Function

NRD1 is a member of the metallopeptidases conserved from prokaryotes to eukaryotes (Pierotti et al., 1994). Several mitochondrial peptidases that belong to this family play a role in

(D) Quantification of the on- and off-transients of ERG traces in 1-day-old and 35-day-old $dNrd1^{A}$ clones in PRs and 35-day-old $dNrd1^{A}$ clones expressing human *NRD1* cDNA. Error bars indicate SEM. p values were calculated using Student's t test. **$p < 0.01$. n.s. indicates not statistically significant.

(E) Familial segregation of the *OGDHL* variant (Chr10:50946295_G>A; OGDHL: NM_018245:exon18:c.C2333T:p.S778L). The *OGDHL* variant is homozygous in the proband and heterozygous in the parents and an unaffected sibling.

(F) Schematic of protein domains of OGDHL and amino acid sequences around S778L. Dotted box (red) indicates a serine residue (red asterisk) that is mutated in patient 2. Arrow (red) indicates a catalytic histidine.

(G) A T1 sagittal MRI image from patient 2 done at age 6 years showing a severely hypoplastic corpus callosum (green arrow) as well as an abnormal cerebellum (green asterisk). A control MRI image T1 sagittal sequence from a 5-year-old child, who was evaluated by neurology for migraine headaches, showing a normal cerebellum and corpus callosum.

(H) A schematic of the generation of *dOgdh-T2A-Gal4* by Recombinase-Mediated Cassette Exchange (RMCE), and the translation of a Gal4 protein by a ribosomal skipping mechanism. The location of the MiMIC insertion *MI06026* is indicated by the red triangle. The T2A-Gal4 cassette consists of a splice acceptor (SA, light gray) followed by a linker (L, dark gray), a ribosomal skipping T2A peptide sequence (red), a Gal4 coding sequence (pale purple), a polyadenylation signal (pA, turquoise), and a splice donor (SD, light gray). Two inverted *attB* sites (blue) are positioned at the 5′ and 3′ end of the cassette.

(I) Left: complementation test results of *dOgdh-T2A-Gal4* alleles. +, complement; –, failure to complement. *dOgdh-T2A-Gal4* complements the original MiMIC insertion (*MI06026*) that is not mutagenic (as it is inserted in the reverse orientation to the gene). *dOgdh-T2A-Gal4* fails to complement a deficiency (*Df(3L)ED4674*) that lacks the *dOgdh* locus. These data indicate that *dOgdh-T2A-Gal4* is a loss-of-function mutant. Right: *dOgdh* lethality can be rescued by expression of wild-type DOGDH or its human homolog, but not by the mutant forms. Gal4 expression from *dOgdh-T2A-Gal4* allowed *dOgdh*, $dOgdh^{S793L}$, *OGDH*, or $OGDH^{S791L}$ to be expressed in *dOgdh* mutant background. See also Figure S6.

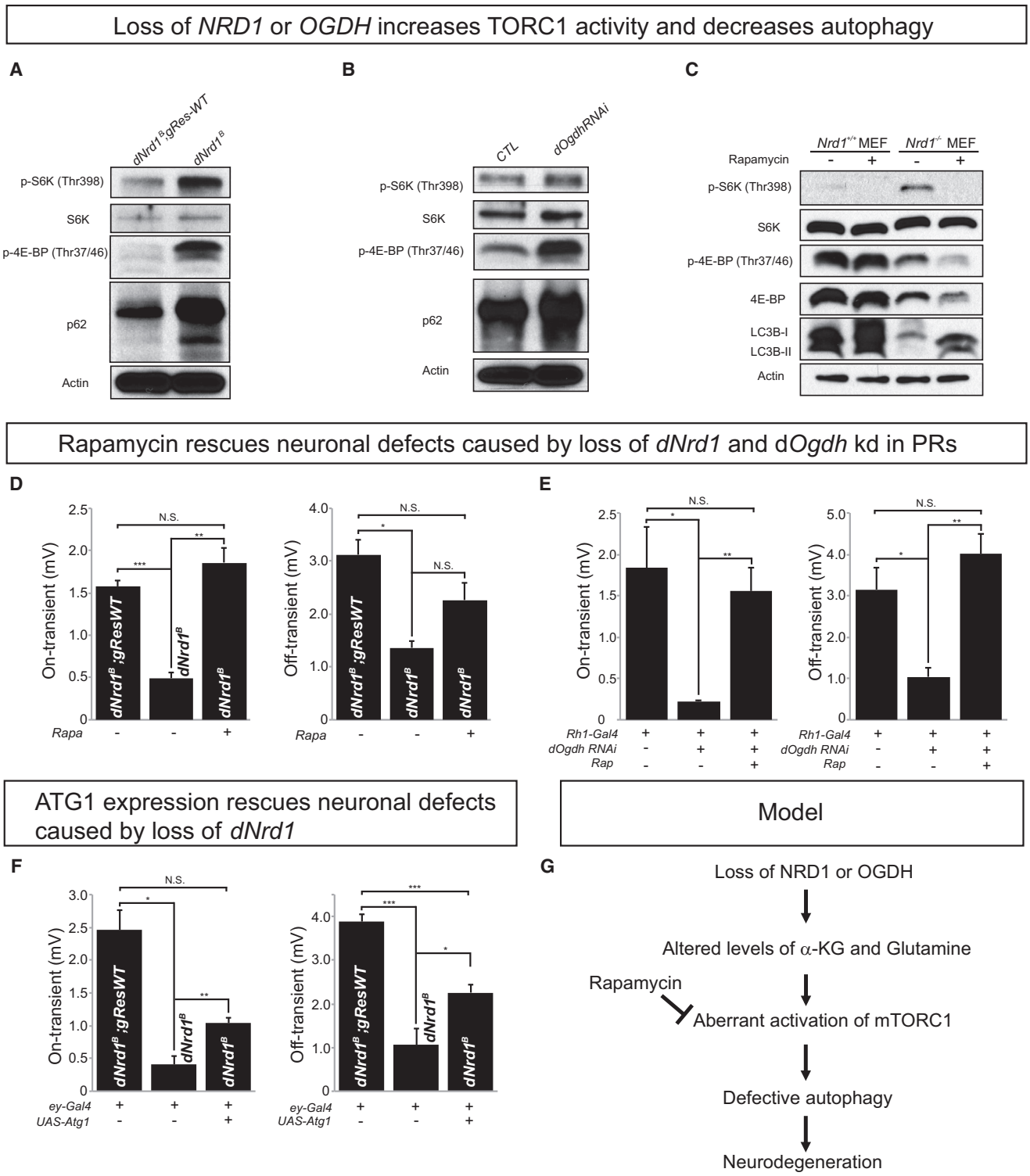

Figure 7. Loss of NRD1 or OGDH Leads to an Increase in TORC1 Activity and Decreases Autophagy

(A and B) Western blots for the levels of phospho-S6K, S6K, phospho-4E-BP, p62, and Actin in *dNrd1* mutants ($dNrd1^{B}$) and its control (A) and in *dOgdh RNAi* (*Act-Gal4/UAS-dOgdh RNAi*) and control animals (*UAS-dOgdh RNAi*/+) (B).

(C) Western blots for the levels of phospho-S6K, S6K, phospho-4E-BP, 4E-BP, LC3B, and Actin in $Nrd1^{ko}$ MEFs ($mNrd1^{-/-}$) and wild-type MEFs ($mNrd1^{+/+}$) with or without rapamycin (100 nM).

(legend continued on next page)

removal of the MTS of nuclear-encoded mitochondrial proteins upon import into mitochondria (Hawlitschek et al., 1988). Loss of these genes causes an accumulation of unprocessed forms of mitochondrial proteins (Mossmann et al., 2014). We, therefore, initially hypothesized that NRD1 plays a role in processing the MTS of TCA cycle enzymes. However, western blot data of OGDH and CS in *mNrd1*$^{-/-}$ MEFs did not show an alteration in molecular weight and did not support this hypothesis (Figure 4I). Instead, our IP/MS experiment in *Drosophila* showed that DNRD1 interacts with DOGDH and several mitochondrial chaperones (Figure 5A). These findings led us to hypothesize that NRD1 is involved in folding and/or stability of OGDH. Indeed, the following observations support this hypothesis. First, NRD1 is required for the activity of OGDH in both fly and MEFs (Figures 4C and 4J). Second, loss of *mNrd1* increases OGDH protein levels in MEFs, while its loss results in a decrease in DOGDH protein levels in *Drosophila* (Figures 4G and 4I). Third, DNRD1 interacts directly or indirectly with numerous chaperones based on IP/MS (Figure 5A; Figure S5B) and co-IP (Figures 5C and 5E). Fourth, an in vitro import assay shows that imported DOGDH is much less stable in the mitochondria that lack DNRD1 (Figure 5D). Fifth, DOGDH is more sensitive to heat shock and becomes more aggregated in the absence of DNRD1 (Figure 5F). Lastly, DNRD1 partially protects DOGDH-Rluc from denaturation under heat shock (Figure 5G). Altogether, our data indicate that NRD1 acts as a mitochondrial chaperone and/or co-chaperone for OGDH.

Loss of NRD1 and OGDH Leads to an Activation of TORC1 and a Decrease in Autophagy

Loss of NRD1 or OGDH alters the profiles of metabolites, including a significant elevation of α-KG. α-KG has been shown to differentially affect mTOR activity in different contexts. Durán et al. (2012) showed that glutamine or its glutaminolysis product, α-KG, activates mTORC1 in a Rag-dependent manner. They also documented that a decrease in α-KG induces autophagy in human cells. However, α-KG was documented to inhibit TOR and enhance autophagy through inhibition of ATP synthase (Chin et al., 2014). We find that loss of *dNrd1* and *mNrd1* causes an elevation of α-KG and glutamine, an increase in TORC1/mTORC1 activity, and a decrease in autophagy (Figures 7A and 7C). Similarly, we observe that loss of *dOgdh* enhances TORC1 signaling and leads to a decrease in autophagy (Figure 7B). In addition, loss of *dNrd1* does not interfere with ATP production (Figure 3E), which may be achieved by TORC1-mediated translational activation of a subset of nuclear-encoded mitochondrial proteins that include subunits of complex I (CI) and complex V (CV) (Morita et al., 2013). Hence, our data are consistent with the observations described in Durán et al. (2012).

Loss of NRD1 and OGDH Leads to an Increase in Lysine Levels

In addition to an elevation of α-KG, loss of *NRD1* or *OGDH* also exhibits a very similar metabolic profile for amino acids, including an elevation of lysine levels (Figures S4A and S4B), which suggests that loss of *NRD1* or *OGDH* may impair one or more enzymes in the lysine catabolic pathway. α-KGDHc has been shown to decarboxylate α-ketoadipic acid (α-KA), an intermediate in the lysine degradation pathway (Hirashima et al., 1967; Kanzaki et al., 1969), consistent with the elevated levels of lysine. Interestingly, patients with mutations in *dehydrogenase E1 and transketolase domain containing 1* (*DHTKD1*), another OGDH-like enzyme (Bunik and Degtyarev, 2008), fail to break down lysine and have elevated levels of α-KA (Danhauser et al., 2012). However, they present with milder intellectual disability and milder symptoms compared to the *NRD1* and *OGDHL* patients (Danhauser et al., 2012). Together, these observations indicate that defects in lysine metabolism are unlikely to be associated with the observed phenotypes, but they may exacerbate phenotypes associated with elevated levels of α-KG in *NRD1* and *OGDHL* patients.

Rare Variants in NRD1 or OGDHL Are Associated with Progressive Loss of Neurological Function in Human

Our data show that loss of NRD1 or OGDH causes an α-KGDHc enzymatic deficiency. In flies, the phenotypes associated with the loss of either protein are very similar as they lead to a very slow, progressive neurodegeneration that is not observed in most mitochondrial mutants (Jaiswal et al., 2015; Liu et al., 2015). In mice, loss of *mNrd1* also causes a slow progression of neurological phenotypes, including impairment of motor coordination and balance, impaired memory, a thin cerebral cortex, and myelination defects in the corpus callosum (Ohno et al., 2009). A number of parallels can be drawn between the phenotypes of patients with homozygous deleterious variants in *NRD1* or *OGDHL*. They both displayed developmental defects at ~1 year of age and progressive neurodegenerative features, including acquired microcephaly, cerebellar volume loss, ataxia, motor impairment, severe intellectual disability, and inability to speak (Table S3). In these families, *NRD1* and *OGDHL* were the best candidate genes from the WES, and using flies, we experimentally demonstrated that the variants in both cases were functionally deleterious, suggesting that these two variants may be linked to the pathogenesis (Figures 6D and

(D) Quantification of the on- and off-transients of ERGs in 35-day-old *dNrd1*^{B} mutant clones in PRs with or without treatment of 3 μM rapamycin and control PRs (*dNrd1*^{B}*;gRes-WT*).

(E) Quantification of the on- and off-transients of ERGs in 28-day-old PRs, where *dOgdh* is knocked down by RNAi (*Rh1-Gal4/UAS-dOgdh RNAi*) with or without treatment of 3 μM rapamycin and control PRs (*Rh-1-Gal4/UAS-empty vector*).

(F) Quantification of the on- and off-transients of ERGs in 35-day-old *dNrd1*^{B} mutant clones in PRs with or without expressing *Atg1* (*ey-Gal4 > UAS-Atg1*) and control PRs (*dNrd1*^{B}*;gRes-WT*). Error bars indicate SEM in (D)–(F). p values were calculated using Student's t test. *p < 0.05, **p < 0.01, ***p < 0.001. n.s. indicates not statistically significant.

(G) Model of neurodegeneration in *NRD1* or *OGDH* mutants: loss of *NRD1* or *OGDH* leads to an elevation of α-KG and glutamine, which induces aberrant activation of mTORC1. Hyperactive mTORC1 signaling causes a decrease in autophagy, which leads to neurodegeneration. Inhibiting mTORC1 activity by treatment of rapamycin rescues neuronal defects in *NRD1* and *OGDH* mutants. See also Figure S7.

6I; Figure S1C). Identification of other patients with deleterious variants in *NRD1* or *OGDHL* will be helpful to further link these genes to the observed phenotypes.

Hyperactivation of mTOR and Other Human Diseases

Our data show that loss of *dNrd1* or *dOgdh* cause neurodegeneration through a hyperactivation of TORC1 and a subsequent decrease in autophagy in flies (Figure 7). Interestingly, hyperactivation of mTOR signaling has also been associated with other human diseases, and suppression of mTOR signaling using mTOR-inhibiting compounds has been shown to be effective in several trials (Crino, 2016; Mirzaa et al., 2016; Pascual, 2016). For example, everolimus, an inhibitor of mTORC1, is approved for treatment of tuberous sclerosis complex-associated subependymal giant cell astrocytomas (Franz et al., 2013). Given that feeding rapamycin to flies that lack *dNrd1* or *dOgdh* partially suppresses the neurodegenerative phenotype, treatment with mTORC1 inhibitors may be a therapeutic avenue for patients with mutations in *NRD1* or *OGDHL*.

In summary, we identify a previously undocumented function of NRD1 in mitochondria in flies and mice. We show that NRD1 binds to and chaperones OGDH, a key enzyme in the TCA cycle. In the absence of NRD1, OGDH is misfolded, leading to an upregulation of a key metabolite, α-KG. Loss of *dNrd1* or *dOgdh* in flies, or loss of *NRD1* or *OGDHL* in humans, is associated with progressive neurodegenerative phenotypes with striking similarities. We further show that elevated levels of α-KG activate TORC1/mTORC1 and decrease autophagy. Consistent with these findings, some aspects of the neurodegenerative phenotypes caused by a decrease in DNRD1 or DOGDH activity can be rescued by providing rapamycin to the flies. Our data provide compelling evidence that intertwining cross species genomic approaches in species as diverse as *Drosophila* and human provide a solid foundation to unravel potential molecular pathogenic mechanisms.

EXPERIMENTAL PROCEDURES

Fly Strains and Maintenance

dNrd1$^{\text{mutants}}$ (*mut* = A,B,C,D) – y^1 *w* dNrd1*^{mut} *P{neoFRT}19A/FM7c*, *Kr-Gal4*, *UAS-GFP*, and X chromosome isogenized control flies – y^1 *w* P{neoFRT}19A* (WT in figures) were generated and mapped as previously described (Haelterman et al., 2014; Yamamoto et al., 2014). For eye mosaic experiments, y^1 *w* dNrd1*$^{A\ or\ B}$, *P{neoFRT}19A/FM7c*, *Kr-Gal4*, *UAS-GFP* were crossed with *y w cl(1) P{neoFRT}19A/Dp(1;Y)y*$^{+}$*; ey-FLP*. *dOgdh-GFP* was generated as previously described (Nagarkar-Jaiswal et al., 2015). *da-Gal4* (RRID: BDSC_55850), *C57-Gal4* (a gift from Vivian Budnik), *D42-Gal4* (RRID: BDSC_8816), *Actin-Gal4, w*^{1118}*; Dp(1;3)DC245, PBac{DC245}VK00033*, *Df(3L) ED4674* (RRID: BDSC_30363), and *VALIUM20-EGFP-shRNA* (RRID: BDSC_41552) were obtained from the Bloomington *Drosophila* Stock Center. *dOgdh RNAi* lines (v12778 [RRID: FlyBase_FBst0450668] for ERG assay; v50393 [RRID: FlyBase_FBst0469014] for metabolic profiling) were obtained from the Vienna *Drosophila* Resource Center (Dietzl et al., 2007). *Mdh2-myc* genomic rescue flies were generously provided by Carl Thummel (Wang et al., 2010). All flies were maintained at room temperature (21°C). Crosses were kept at 25°C.

Aggregation Assay

An aggregation assay was performed as previously described (Bender et al., 2011). Briefly, a total of 200 μg isolated mitochondria were resuspended in 400 μL of an aggregation assay buffer (250 mM sucrose, 10 mM MOPS/KOH [pH 7.2], 3 mM $MgCl_2$, 80 mM KCl, 2 mM NADH, and 1 mM ATP). Mitochondria in buffer were divided into two tubes: one tube was incubated at 25°C and the other tube was incubated at 42°C. After incubation, mitochondria were isolated in mitochondria isolation buffer by centrifugation at 8,000 × *g* for 10 min at 4°C. Isolated mitochondria were lysed in 100 μL of lysis buffer (0.5% Triton X-100, 30 mM Tris [pH 7.4], 200 mM KCl, and 5 mM EDTA) containing cOmplete protease inhibitor (Roche) and subjected to ultracentrifugation at 125 kg for 30 min at 4°C. Supernatants were removed and the pellets were re-extracted by vigorous shaking in the lysis buffer. Supernatants and pellets were analyzed by western blot using anti-Flag antibody (Sigma-Aldrich Cat# F1804, RRID: AB_262044) and anti-ATP5A antibody (Abcam Cat# ab14748, RRID: AB_301447).

Ethics Statement

Informed consent was obtained prior to participation from all subjects or parents of recruited subjects under an Institutional Review Board-approved protocol at Baylor College of Medicine (H-29697) through the Center for Mendelian Genomics[73] or at the University of California in Los Angeles (11-001087).

SUPPLEMENTAL INFORMATION

Supplemental Information includes Supplemental Experimental Procedures, seven figures, and three tables and can be found with this article online at http://dx.doi.org/10.1016/j.neuron.2016.11.038.

AUTHOR CONTRIBUTIONS

W.H.Y. and H.J.B. conceived and designed the project. W.H.Y. designed and conducted most experiments and analyzed the data. H.S., M.J., and S.Y. performed the genetic screen and mapping. N.A.H. mapped several alleles. S.N.-J. generated *dOgdh-GFP* reagent. N.P., V.P., and A.S. performed metabolomic profiling and analysis. T.D. and B.H.G. performed mitochondrial copy number and ETC assays. E.N. and M.O. generated *Nrd1* knockout MEF reagent. D.M.M. performed WES. J.H. interpreted MRI data. T.T., A.A., J.C., J.S., V.A.A., and E.K. collected clinical data. M.F.W. and E.K. analyzed clinical and genomic data. V.A.A., S.F.N., E.K., and J.R.L. collected human subjects, performed segregation analysis, and identified the patients. W.H.Y., M.F.W., S.Y., and H.J.B. wrote the manuscript.

ACKNOWLEDGMENTS

We thank L. Duraine, P.-T. Li, and Y. He for technical support; A. Leibfried, A. Ephrussi, and C. Thummel for reagents; Y. Kwon for assistance with bioinformatics; E. Seto for reading the MRI images; K. Venkatachalam and H.-T. Chao for critical reading of this manuscript; and K. Schulze for proofreading. This study was supported by NIH 5R01GM067858, NIH T32 NS043124-11, and the Research Education and Career Horizon Institutional Research and Academic Career Development Award Fellowship 5K12GM084897 (H.S.), the Jan and Dan Duncan Neurological Research Institute at Texas Children's Hospital (S.Y.), the CPRIT Metabolomics Core Facility Support Award RP120092 (N.P. and A.S.K.), NCI 2P30CA125123-09 Shared Resources Metabolomics core, funds from Dan L. Duncan Cancer Center (DLDCC), Alkek Center for Molecular Discovery (A.S. and N.P.), Mass Spectrometry COE by Agilent (A.S. and N.P.), NIH R01GM098387 (B.H.G.), the Japanese research grants (26293068, 26670139, and 26116715), a research program of the P-Direct from the MEXT of Japan (E.N.), and NIH K08NS076547 and R01NS058529 funded by NINDS (M.F.W. and J.R.L., respectively). We acknowledge support of the NIH (1RC4GM096355), the Robert A. and Renee E. Belfer Family Foundation, the Huffington Foundation, and Target ALS to H.J.B. H.J.B. is an Investigator of the Howard Hughes Medical Institute. This work was also supported in part by the National institute of Neurological Disease and Stroke (NINDS) R01NS058529 (J.R.L.). The Baylor-Hopkins Center for Mendelian Genomics is funded jointly by the US National Human Genome Research Institute (NHGRI) and National Heart, Lung, and Blood Institute (NHLBI) grant U54HG006542. Confocal microscopy was supported by the Baylor College of Medicine IDDRC grant number 1U54 HD083092 from the Eunice

Kennedy Shriver National Institute of Child Health & Human Development (U54HD083092).

J.R.L. has stock ownership in 23andMe and Lasergen, is a paid consultant for Regeneron Pharmaceuticals, and is a coinventor on multiple United States and European patents related to molecular diagnostics for inherited neuropathies, eye diseases, and bacterial genomic fingerprinting. The Baylor College of Medicine derives revenue from the chromosomal microarray analysis and clinical exome sequencing offered by the Baylor Genetics Laboratory (http://www.bmgl.com/BMGL/Default.aspx).

Received: February 24, 2016
Revised: August 21, 2016
Accepted: November 14, 2016
Published: December 22, 2016

REFERENCES

Adzhubei, I.A., Schmidt, S., Peshkin, L., Ramensky, V.E., Gerasimova, A., Bork, P., Kondrashov, A.S., and Sunyaev, S.R. (2010). A method and server for predicting damaging missense mutations. Nat. Methods *7*, 248–249.

Ali, Y.O., Allen, H.M., Yu, L., Li-Kroeger, D., Bakhshizadehmahmoudi, D., Hatcher, A., McCabe, C., Xu, J., Bjorklund, N., Taglialatela, G., et al. (2016). NMNAT2:HSP90 complex mediates Proteostasis in Proteinopathies. PLoS Biol. *14*, e1002472.

Barcelo, H., and Stewart, M.J. (2002). Altering Drosophila S6 kinase activity is consistent with a role for S6 kinase in growth. Genesis *34*, 83–85.

Bellen, H.J., and Yamamoto, S. (2015). Morgan's legacy: fruit flies and the functional annotation of conserved genes. Cell *163*, 12–14.

Bender, T., Lewrenz, I., Franken, S., Baitzel, C., and Voos, W. (2011). Mitochondrial enzymes are protected from stress-induced aggregation by mitochondrial chaperones and the Pim1/LON protease. Mol. Biol. Cell *22*, 541–554.

Bunik, V.I., and Degtyarev, D. (2008). Structure-function relationships in the 2-oxo acid dehydrogenase family: substrate-specific signatures and functional predictions for the 2-oxoglutarate dehydrogenase-like proteins. Proteins *71*, 874–890.

Bunik, V., Kaehne, T., Degtyarev, D., Shcherbakova, T., and Reiser, G. (2008). Novel isoenzyme of 2-oxoglutarate dehydrogenase is identified in brain, but not in heart. FEBS J. *275*, 4990–5006.

Burté, F., Carelli, V., Chinnery, P.F., and Yu-Wai-Man, P. (2015). Disturbed mitochondrial dynamics and neurodegenerative disorders. Nat. Rev. Neurol. *11*, 11–24.

Chesneau, V., Pierotti, A.R., Prat, A., Gaudoux, F., Foulon, T., and Cohen, P. (1994). N-arginine dibasic convertase (NRD convertase): a newcomer to the family of processing endopeptidases. An overview. Biochimie *76*, 234–240.

Chin, R.M., Fu, X., Pai, M.Y., Vergnes, L., Hwang, H., Deng, G., Diep, S., Lomenick, B., Meli, V.S., Monsalve, G.C., et al. (2014). The metabolite α-ketoglutarate extends lifespan by inhibiting ATP synthase and TOR. Nature *510*, 397–401.

Chong, J.X., Buckingham, K.J., Jhangiani, S.N., Boehm, C., Sobreira, N., Smith, J.D., Harrell, T.M., McMillin, M.J., Wiszniewski, W., Gambin, T., et al.; Centers for Mendelian Genomics (2015). The genetic basis of Mendelian phenotypes: discoveries, challenges, and opportunities. Am. J. Hum. Genet. *97*, 199–215.

Claros, M.G., and Vincens, P. (1996). Computational method to predict mitochondrially imported proteins and their targeting sequences. Eur. J. Biochem. *241*, 779–786.

Crino, P.B. (2016). The mTOR signalling cascade: paving new roads to cure neurological disease. Nat. Rev. Neurol. *12*, 379–392.

Danhauser, K., Sauer, S.W., Haack, T.B., Wieland, T., Staufner, C., Graf, E., Zschocke, J., Strom, T.M., Traub, T., Okun, J.G., et al. (2012). DHTKD1 mutations cause 2-aminoadipic and 2-oxoadipic aciduria. Am. J. Hum. Genet. *91*, 1082–1087.

Diao, F., Ironfield, H., Luan, H., Diao, F., Shropshire, W.C., Ewer, J., Marr, E., Potter, C.J., Landgraf, M., and White, B.H. (2015). Plug-and-play genetic access to drosophila cell types using exchangeable exon cassettes. Cell Rep. *10*, 1410–1421.

Dietzl, G., Chen, D., Schnorrer, F., Su, K.-C., Barinova, Y., Fellner, M., Gasser, B., Kinsey, K., Oppel, S., Scheiblauer, S., et al. (2007). A genome-wide transgenic RNAi library for conditional gene inactivation in Drosophila. Nature *448*, 151–156.

Durán, R.V., Oppliger, W., Robitaille, A.M., Heiserich, L., Skendaj, R., Gottlieb, E., and Hall, M.N. (2012). Glutaminolysis activates Rag-mTORC1 signaling. Mol. Cell *47*, 349–358.

Franceschini, A., Szklarczyk, D., Frankild, S., Kuhn, M., Simonovic, M., Roth, A., Lin, J., Minguez, P., Bork, P., von Mering, C., and Jensen, L.J. (2013). STRING v9.1: protein-protein interaction networks, with increased coverage and integration. Nucleic Acids Res. *41*, D808–D815.

Franz, D.N., Belousova, E., Sparagana, S., Bebin, E.M., Frost, M., Kuperman, R., Witt, O., Kohrman, M.H., Flamini, J.R., Wu, J.Y., et al. (2013). Efficacy and safety of everolimus for subependymal giant cell astrocytomas associated with tuberous sclerosis complex (EXIST-1): a multicentre, randomised, placebo-controlled phase 3 trial. Lancet *381*, 125–132.

Fumagalli, P., Accarino, M., Egeo, A., Scartezzini, P., Rappazzo, G., Pizzuti, A., Avvantaggiato, V., Simeone, A., Arrigo, G., Zuffardi, O., et al. (1998). Human NRD convertase: a highly conserved metalloendopeptidase expressed at specific sites during development and in adult tissues. Genomics *47*, 238–245.

Haelterman, N.A., Jiang, L., Li, Y., Bayat, V., Sandoval, H., Ugur, B., Tan, K.L., Zhang, K., Bei, D., Xiong, B., et al. (2014). Large-scale identification of chemically induced mutations in Drosophila melanogaster. Genome Res. *24*, 1707–1718.

Hawlitschek, G., Schneider, H., Schmidt, B., Tropschug, M., Hartl, F.U., and Neupert, W. (1988). Mitochondrial protein import: identification of processing peptidase and of PEP, a processing enhancing protein. Cell *53*, 795–806.

Hiraoka, Y., Matsuoka, T., Ohno, M., Nakamura, K., Saijo, S., Matsumura, S., Nishi, K., Sakamoto, J., Chen, P.M., Inoue, K., et al. (2014). Critical roles of nardilysin in the maintenance of body temperature homoeostasis. Nat. Commun. *5*, 3224.

Hirashima, M., Hayakawa, T., and Koike, M. (1967). Mammalian alpha-keto acid dehydrogenase complexes. II. An improved procedure for the preparation of 2-oxoglutarate dehydrogenase complex from pig heart muscle. J. Biol. Chem. *242*, 902–907.

Horwich, A.L., Kalousek, F., Mellman, I., and Rosenberg, L.E. (1985). A leader peptide is sufficient to direct mitochondrial import of a chimeric protein. EMBO J. *4*, 1129–1135.

Hospital, V., Chesneau, V., Balogh, A., Joulie, C., Seidah, N.G., Cohen, P., and Prat, A. (2000). N-arginine dibasic convertase (nardilysin) isoforms are soluble dibasic-specific metalloendopeptidases that localize in the cytoplasm and at the cell surface. Biochem. J. *349*, 587–597.

Huergo, L.F., and Dixon, R. (2015). The emergence of 2-Oxoglutarate as a master regulator metabolite. Microbiol. Mol. Biol. Rev. *79*, 419–435.

Jaiswal, M., Haelterman, N.A., Sandoval, H., Xiong, B., Donti, T., Kalsotra, A., Yamamoto, S., Cooper, T.A., Graham, B.H., and Bellen, H.J. (2015). Impaired mitochondrial energy production causes light-induced photoreceptor degeneration independent of oxidative stress. PLoS Biol. *13*, e1002197.

Johri, A., and Beal, M.F. (2012). Mitochondrial dysfunction in neurodegenerative diseases. J. Pharmacol. Exp. Ther. *342*, 619–630.

Kanzaki, T., Hayakawa, T., Hamada, M., Fukuyoshi, Y., and Koike, M. (1969). Mammalian alpha-keto acid dehydrogenase complexes. IV. Substrate specificities and kinetic properties of the pig heart pyruvate and 2-oxyoglutarate dehydrogenase complexes. J. Biol. Chem. *244*, 1183–1187.

Karaca, E., Harel, T., Pehlivan, D., Jhangiani, S.N., Gambin, T., Coban Akdemir, Z., Gonzaga-Jauregui, C., Erdin, S., Bayram, Y., Campbell, I.M., et al. (2015). Genes that Affect Brain Structure and Function Identified by Rare Variant Analyses of Mendelian Neurologic Disease. Neuron *88*, 499–513.

Kumar, P., Henikoff, S., and Ng, P.C. (2009). Predicting the effects of coding non-synonymous variants on protein function using the SIFT algorithm. Nat. Protoc. *4*, 1073–1081.

Laplante, M., and Sabatini, D.M. (2012). mTOR signaling. Cold Spring Harb. Perspect. Biol. *4*, a011593.

Lee, H., Deignan, J.L., Dorrani, N., Strom, S.P., Kantarci, S., Quintero-Rivera, F., Das, K., Toy, T., Harry, B., Yourshaw, M., et al. (2014). Clinical exome sequencing for genetic identification of rare Mendelian disorders. JAMA *312*, 1880–1887.

Lek, M., Karczewski, K.J., Minikel, E.V., Samocha, K.E., Banks, E., Fennell, T., O'Donnell-Luria, A.H., Ware, J.S., Hill, A.J., Cummings, B.B., et al.; Exome Aggregation Consortium (2016). Analysis of protein-coding genetic variation in 60,706 humans. Nature *536*, 285–291.

Liu, L., Zhang, K., Sandoval, H., Yamamoto, S., Jaiswal, M., Sanz, E., Li, Z., Hui, J., Graham, B.H., Quintana, A., and Bellen, H.J. (2015). Glial lipid droplets and ROS induced by mitochondrial defects promote neurodegeneration. Cell *160*, 177–190.

Ma, Z., Chow, K.M., Yao, J., and Hersh, L.B. (2004). Nuclear shuttling of the peptidase nardilysin. Arch. Biochem. Biophys. *422*, 153–160.

Menzies, F.M., Fleming, A., and Rubinsztein, D.C. (2015). Compromised autophagy and neurodegenerative diseases. Nat. Rev. Neurosci. *16*, 345–357.

Mirzaa, G.M., Campbell, C.D., Solovieff, N., Goold, C.P., Jansen, L.A., Menon, S., Timms, A.E., Conti, V., Biag, J.D., Olds, C., et al. (2016). Association of MTOR mutations with developmental brain disorders, including Megalencephaly, Focal Cortical Dysplasia, and Pigmentary Mosaicism. JAMA Neurol. *73*, 836–845.

Morita, M., Gravel, S.-P., Chénard, V., Sikström, K., Zheng, L., Alain, T., Gandin, V., Avizonis, D., Arguello, M., Zakaria, C., et al. (2013). mTORC1 controls mitochondrial activity and biogenesis through 4E-BP-dependent translational regulation. Cell Metab. *18*, 698–711.

Mossmann, D., Vögtle, F.-N., Taskin, A.A., Teixeira, P.F., Ring, J., Burkhart, J.M., Burger, N., Pinho, C.M., Tadic, J., Loreth, D., et al. (2014). Amyloid-β peptide induces mitochondrial dysfunction by inhibition of preprotein maturation. Cell Metab. *20*, 662–669.

Na, U., Yu, W., Cox, J., Bricker, D.K., Brockmann, K., Rutter, J., Thummel, C.S., and Winge, D.R. (2014). The LYR factors SDHAF1 and SDHAF3 mediate maturation of the iron-sulfur subunit of succinate dehydrogenase. Cell Metab. *20*, 253–266.

Nagarkar-Jaiswal, S., Lee, P.T., Campbell, M.E., Chen, K., Anguiano-Zarate, S., Gutierrez, M.C., Busby, T., Lin, W.W., He, Y., Schulze, K.L., et al. (2015). A library of MiMICs allows tagging of genes and reversible, spatial and temporal knockdown of proteins in Drosophila. eLife *4*, e05338.

Ng, P.C., and Henikoff, S. (2003). SIFT: Predicting amino acid changes that affect protein function. Nucleic Acids Res. *31*, 3812–3814.

Nishi, E., Hiraoka, Y., Yoshida, K., Okawa, K., and Kita, T. (2006). Nardilysin enhances ectodomain shedding of heparin-binding epidermal growth factor-like growth factor through activation of tumor necrosis factor-alpha-converting enzyme. J. Biol. Chem. *281*, 31164–31172.

Ohno, M., Hiraoka, Y., Matsuoka, T., Tomimoto, H., Takao, K., Miyakawa, T., Oshima, N., Kiyonari, H., Kimura, T., Kita, T., and Nishi, E. (2009). Nardilysin regulates axonal maturation and myelination in the central and peripheral nervous system. Nat. Neurosci. *12*, 1506–1513.

Owen, O.E., Kalhan, S.C., and Hanson, R.W. (2002). The key role of anaplerosis and cataplerosis for citric acid cycle function. J. Biol. Chem. *277*, 30409–30412.

Pascual, J.M. (2016). Genetic gradients in epileptic brain malformations. JAMA Neurol. *73*, 787.

Pfanner, N., Craig, E.A., and Hönlinger, A. (1997). Mitochondrial preprotein translocase. Annu. Rev. Cell Dev. Biol. *13*, 25–51.

Pickrell, A.M., and Youle, R.J. (2015). The roles of PINK1, parkin, and mitochondrial fidelity in Parkinson's disease. Neuron *85*, 257–273.

Pierotti, A.R., Prat, A., Chesneau, V., Gaudoux, F., Leseney, A.M., Foulon, T., and Cohen, P. (1994). N-arginine dibasic convertase, a metalloendopeptidase as a prototype of a class of processing enzymes. Proc. Natl. Acad. Sci. USA *91*, 6078–6082.

Rizzuto, R., Brini, M., Pizzo, P., Murgia, M., and Pozzan, T. (1995). Chimeric green fluorescent protein as a tool for visualizing subcellular organelles in living cells. Curr. Biol. *5*, 635–642.

Rowley, N., Prip-Buus, C., Westermann, B., Brown, C., Schwarz, E., Barrell, B., and Neupert, W. (1994). Mdj1p, a novel chaperone of the DnaJ family, is involved in mitochondrial biogenesis and protein folding. Cell *77*, 249–259.

Rustin, P., Bourgeron, T., Parfait, B., Chretien, D., Munnich, A., and Rötig, A. (1997). Inborn errors of the Krebs cycle: a group of unusual mitochondrial diseases in human. Biochim. Biophys. Acta *1361*, 185–197.

Sobreira, N., Schiettecatte, F., Valle, D., and Hamosh, A. (2015). GeneMatcher: a matching tool for connecting investigators with an interest in the same gene. Hum. Mutat. *36*, 928–930.

Van Vranken, J.G., Bricker, D.K., Dephoure, N., Gygi, S.P., Cox, J.E., Thummel, C.S., and Rutter, J. (2014). SDHAF4 promotes mitochondrial succinate dehydrogenase activity and prevents neurodegeneration. Cell Metab. *20*, 241–252.

Venken, K.J.T., Carlson, J.W., Schulze, K.L., Pan, H., He, Y., Spokony, R., Wan, K.H., Koriabine, M., de Jong, P.J., White, K.P., et al. (2009). Versatile P[acman] BAC libraries for transgenesis studies in Drosophila melanogaster. Nat. Methods *6*, 431–434.

Venken, K.J.T., Popodi, E., Holtzman, S.L., Schulze, K.L., Park, S., Carlson, J.W., Hoskins, R.A., Bellen, H.J., and Kaufman, T.C. (2010). A molecularly defined duplication set for the X chromosome of Drosophila melanogaster. Genetics *186*, 1111–1125.

Venken, K.J.T., Schulze, K.L., Haelterman, N.A., Pan, H., He, Y., Evans-Holm, M., Carlson, J.W., Levis, R.W., Spradling, A.C., Hoskins, R.A., and Bellen, H.J. (2011). MiMIC: a highly versatile transposon insertion resource for engineering Drosophila melanogaster genes. Nat. Methods *8*, 737–743.

Verstreken, P., Koh, T.W., Schulze, K.L., Zhai, R.G., Hiesinger, P.R., Zhou, Y., Mehta, S.Q., Cao, Y., Roos, J., and Bellen, H.J. (2003). Synaptojanin is recruited by endophilin to promote synaptic vesicle uncoating. Neuron *40*, 733–748.

Vinayagam, A., Hu, Y., Kulkarni, M., Roesel, C., Sopko, R., Mohr, S.E., and Perrimon, N. (2013). Protein complex-based analysis framework for high-throughput data sets. Sci. Signal. *6*, rs5.

Wang, L., Lam, G., and Thummel, C.S. (2010). Med24 and Mdh2 are required for Drosophila larval salivary gland cell death. Dev. Dyn. *239*, 954–964.

Yamamoto, S., Jaiswal, M., Charng, W.L., Gambin, T., Karaca, E., Mirzaa, G., Wiszniewski, W., Sandoval, H., Haelterman, N.A., Xiong, B., et al. (2014). A drosophila genetic resource of mutants to study mechanisms underlying human genetic diseases. Cell *159*, 200–214.